SPECTROSCOPIC AND ANALYTICAL CHARACTERIZATION OF THE DISTRIBUTION OF IRON IN INTACT MITOCHONDRIA FROM *Saccharomyces cerevisiae*

A Dissertation

by

BRANDON NEAL HUDDER

Submitted to the Office of Graduate Studies of
Texas A&M University
in partial fulfillment of the requirements for the degree of

DOCTOR OF PHILOSOPHY

August 2006

Major Subject: Chemistry

SPECTROSCOPIC AND ANALYTICAL CHARACTERIZATION OF THE DISTRIBUTION OF IRON IN INTACT MITOCHONDRIA FROM *Saccharomyces cerevisiae*

A Dissertation

by

BRANDON NEAL HUDDER

Submitted to the Office of Graduate Studies of
Texas A&M University
in partial fulfillment of the requirements for the degree of

DOCTOR OF PHILOSOPHY

Approved by:

Chair of Committee, Paul A. Lindahl
Committee Members, Marcetta Y. Darensbourg
Edward D. Harris
Simon W. North
Head of Department, Emile A. Schweikert

August 2006

Major Subject: Chemistry

ABSTRACT

Spectroscopic and Analytical Characterization of the Distribution of Iron in Intact Mitochondria from *Saccharomyces cerevisiae*. (August 2006)

Brandon Neal Hudder, B. A., University of West Georgia

Chair of Advisory Committee: Dr. Paul A. Lindahl

Electron paramagnetic resonance (EPR) and Mössbauer spectroscopy were used to examine the distribution of iron in mitochondria from *Saccharomyces cerevisiae*. These organelles were packed into EPR and Mössbauer cuvettes, affording spectra with unprecedented signal/noise ratios. EPR spectra of as-isolated intact mitochondria exhibited fourteen distinct signals, some of which were assigned according to previously reported *g*-values obtained using isolated proteins. Signals from adventitious manganese (II) and iron (III) were largely removed when mitochondria were isolated in buffers supplemented with the metal chelators EDTA or EGTA. Signals were simulated and intensities were quantified to afford spin concentrations and estimates of the concentration of EPR-active species in mitochondria. The effects of treating samples with chemical modifiers were examined. Packed samples were analyzed for protein and metal content, affording averaged values of 50 mg/mL [protein], 590 μM [Fe], 340 μM [Cu], and 17 μM [Mn].

^{57}Fe-enriched intact mitochondria isolated in the presence of metal chelators exhibited Mössbauer spectra dominated by three components. Approximately 60% of the ^{57}Fe in the sample gave rise to a quadrupole doublet, most of which was diamagnetic.

The parameters of this doublet are typical of $S = 0$ $[4Fe\text{-}4S]^{2+}$ clusters and $S = 0$ ferrous heme groups. Spectra of samples reduced with dithionite, pH 8.5, suggested that at least half of this doublet arose from $[4Fe\text{-}4S]^{2+}$ clusters. The second major component exhibited in the Mössbauer spectra arose from high-spin ferrous ions (10%-30%). The third major component (15%) came from iron exhibiting magnetic hyperfine interactions and is likely reflected in the Fe-containing species observed by EPR.

The results presented here suggest that mitochondria contain ~ 600 μM of Fe overall, ~ 200 – 400 μM organized as $[4Fe\text{-}4S]^{2+}$ clusters, with about 25 μM due to the $[4Fe\text{-}4S]^{2+}$ cluster of aconitase. Approximately 60 μM – 200 μM of the Fe in mitochondria is high-spin ferrous ions, ~ 40 μM as the Rieske $S = 1/2$ $[2Fe\text{-}2S]^{+}$ cluster of cytochrome bc_1, and ~20 μM as the $S = 1/2$ $[2Fe\text{-}2S]^{+}$ cluster of succinate dehydrogenase. The high-spin ferric hemes of the a_3:Cu_B site of cytochrome oxidase and cytochrome *c* peroxidase each account for ~ 4 μM of Fe.

DEDICATION

I dedicate this work to my family, friends, and God Almighty. My parents, Barry and Nancy, my brother, Eric, my grandparents, Jack and Margaret Hudder, and Ed and Virginia Hitchcock, have always provided me with the encouragement and support one needs to become successful in all facets of life.

ACKNOWLEDGEMENTS

I am indebted to my family and friends who have shaped me both personally and professionally. They have all blessed me with their love and friendship. My childhood friends and companions will always hold a special place in my heart. Michael Robbins, Ryan Kauffman, Timothy Ayers, and Christopher Lane have my eternal gratitude for befriending me during my undergraduate days. My graduate education afforded me further opportunities to make friendships that I hope to carry through the rest of my days, and I would like to particularly thank Jake Wildeson, Jim Donahue, Sergio Gonzalez, B.J. Bench, Thom Kelly, Tom Maguire, Rob North, Eric Schwerdtfeger and Brian Sobkowiak for being true friends during my time in College Station. I was blessed to find the love of my life, Ms. Tara Bolton, while living in College Station. She has shown me the type of unconditional friendship and affection that I had always hoped to find. You have my undying loyalty and love, Tara. Thank you for all that you have done and continue to do for me.

I would like to acknowledge the teachers, coaches, and professors, I was fortunate enough to have in my life. Mr. Rodney Arrington was a teacher and coach who constantly challenged me to give my best in every endeavor, for that I thank him. Professors Joshua Du, Andrew Leavitt, Farooq Khan, and Mr. William Harper were gentlemen who provided me with knowledge, guidance, and friendship. They have my heartfelt appreciation for all they have done for me.

I would not be able to record this work without the assistance, patience, and friendship of Professor Paul Lindahl. In addition to training me as a competent scientist

and critical thinker, Paul provided me with the unique opportunity to inaugurate the mitochondrial systems biology experimental project that seems well on its way to being an enormous success. He has always provided me with helpful tips and insights whenever I reached a stalemate in my research yet never “micromanaged” my project. Paul provided me with unending opportunities, whether it was performing an experiment, designing new tools and repairing laboratory equipment, or challenging me to provide leadership and direction for my labmates. I appreciate everything you have done for me. You’re the best, Paul.

I am indebted to my committee members, Professors Marcetta Darensbourg, Ed Harris, and Simon North as well as my surrogate committee member, Professor Coran Watanabe, for their guidance and patience. I also appreciate the hard work and assistance of my collaborators, Professor Michael Hendrich, Dr. Audria Stubna, and Professor Eckard Münck, all of Carnegie Mellon University, as well as Professor Roland Lill of Philips University (Marburg, FRG). I appreciate the assistance and camaraderie of all of my labmates, particularly Drs. Matt Bramlett, Ivan Surovtsev, and Xiangshi Tan, Mr. Ren Miao, and Ms. Michelle House. I also appreciate the efforts of Professor Art Johnson and Mrs. Holly Cargill for providing instructions on isolating mitochondria. There were numerous other faculty and staff members, including Professors Don Darensbourg and Ray Schaak, who provided me with guidance and friendship during my graduate career.

I would also like to thank the taxpayers of both the great state of Texas and the United States of America for providing the funds that supported me and my research. I

am very grateful to both the National Institutes of Health and the Welch Foundation for providing me with predoctoral training grants.

TABLE OF CONTENTS

Page

TABLE OF CONTENTS

LIST OF FIGURES

LIST OF TABLES

NOMENCLATURE

AAA, amino acid analysis

AAS, atomic absorption spectroscopy

ADP, adenosine diphosphate

Ar, argon

ATP, adenosine triphosphate

Buffer 1 × SH: 0.6 M sorbitol, 20 mM HEPES-KOH, pH 7.4

Buffer 2 × SHP: 1.2 *M* sorbitol, 40 m*M* HEPES-KOH, pH 7.4, 1 mM PMSF

Buffer SP: 1.2 *M* sorbitol, 20 m*M* potassium phosphate, pH 7.4

Buffer TD, 100 m*M* Tris-SO_4. pH 9.4, 10 m*M* DTT

CD, central doublet

CO, carbon monoxide

Cu, copper

Cyt., cytochrome

DD-H_2O, distilled/deionized water

DTT, *D, L*-dithiothreitol

$E°'$, standard thermodynamic reduction potential

EDTA, ethylenediaminetetraacetic acid

EGTA, ethylenebis(oxyethylenenitrilo)tetraacetic acid

EM, electron microscopy

EPR, electron paramagnetic resonance spectroscopy

FC, ferrous component

Fe, iron

Fe/S, iron-sulfur cluster

HCl, hydrochloric acid

HNO_3, nitric acid

ID, inner diameter

IM, inner membrane

IMS, intermembrane space

MM, magnetic material

Mn, manganese

N_2, molecular nitrogen

NHE, normal hydrogen electrode

OD, outer diameter

OM, outer membrane

O_2, molecular oxygen

PMSF, phenylmethylsulfonyl fluoride

QD, quadrupole doublet

QH_2, ubiquinol

ROS, reactive oxygen species

RPM, revolutions per minute

S/N, signal-to-noise

SOD, superoxide dismutase

TEM, transmission electron microscope

Tris-SO_4, tris(hydroxymethyl)aminomethane-SO_4

CHAPTER I

INTRODUCTION

Mitochondria are essential organelles responsible for carrying out a myriad of indispensable cellular processes in eukaryotic cells (1). These organelles are typically represented in textbooks as sausage-shaped entities, approximately 3 μm in length and 1 μm in width, although recent studies have supported the idea of a coordinated tubular network, a "mitochondria superhighway", rather than that of discrete organelles operating *in vivo* (2). Mitochondria are comprised of an outer membrane, an inner membrane (IM), an intermembrane space (IMS), matrix, and cristae, which are protrusions extending from the inner membrane into the matrix. These features provide increased surface area for various reactions and processes carried out in mitochondria, including oxidative phosphorylation.

Many diseases and degradative processes affecting humans can be directly correlated to mitochondrial dysfunction. The process of aging is integrally linked to the oxidative degradation of mitochondria and mitochondrial DNA (3). Diseases and afflictions such as diabetes, heart disease, deafness, blindness and others often result from defects in mitochondrial function and/or loss of mitochondrial DNA (4, 5, 6, 7). Many of these diseases and processes are induced, either directly or indirectly, by abnormal transition metal homeostasis, i.e. the improper processing and assimilation of

---

This dissertation follows the style and format of *Biochemistry*.

iron, copper, and manganese. Approximately two billion people worldwide are affected by iron deficiencies in their diet (8). Friedrich's ataxia, a neurodegenerative disease resulting from mitochondrial iron overload, results in deafness, blindness, heart disease, and ultimately death (9).

Mitochondria from *Saccharomyces cerevisiae*, commonly known as baker's yeast, are the most well studied of these organelles. Among the most recognizable processes performed by mitochondria are oxidative phosphorylation and the citric acid cycle as well as fatty acid, porphyrin/heme and iron-sulfur cluster biosynthesis. All of the aforementioned processes share a common link in that these pathways and processes utilize iron-containing proteins. The most prominent cofactors in these iron-containing proteins are hemes and iron-sulfur clusters.

In mitochondria, hemes can be of three types – *a*, *b*, and *c* – found exclusively in cytochromes of the *a*-, *b*-, *and c*-type, respectively (Figure on page 5). Hemes are found in several mitochondrial proteins, specifically, those involved in either oxidative phosphorylation, the process by which cells obtain ATP from the phosphorylation of ADP, or in their assembly and maintenance. Hemes are inserted into cytochromes, so named for their characteristic absorption bands in the visible portion of the radiant energy spectrum. Several of these proteins are found in the protein complexes that comprise the oxidative phosphorylation pathway. Cytochromes b_H, b_L, and c_1 transfer electrons in the oxidative phosphorylation complex cytochrome bc_1 to cytochrome *c*. Proteins such as cytochrome *c* lyase and cytochrome c_1 lyase are responsible for the insertion of cytochromes *c* and c_1, respectively. The IMS yeast protein Ccp1p is a

peroxidase that reduces hydrogen peroxide to water (10). The synthesis of the organic-based porphyrin macrocycle occurs in both the cytosol and the mitochondrion (11). However, insertion of the iron cofactor into the porphyrin ring occurs exclusively in the mitochondrion and is carried out by ferrochelatase, encoded by the Hem15 gene in *S. cerevisiae* (12, 13).

The synthesis of iron-sulfur (Fe/S) clusters is carried out almost exclusively in mitochondria. The role of iron-sulfur clusters in mitochondrial metabolism and electron transfer has been extensively investigated (14). These cofactors are found in all organisms and perform a multitude of functions. Fe/S clusters are commonly found in [2Fe-2S], [3Fe-4S], and [4Fe-4S] forms (Figure 1-1). They are involved in electron transfer and metabolic processes as well as iron and oxygen sensing (15). Among the most prominent Fe/S cluster containing proteins is the cluster-containing protein of succinate dehydrogenase, which reduces ubiquinone to ubiquinol through the oxidation of $FADH_2$ for entry into the electron transport chain in oxidative phosphorylation. This protein is also charged with converting succinate to fumarate, with the concomitant reduction of FAD to $FADH_2$, in the citric acid cycle. Others include the Rieske protein of the cytochrome bc_1 complex, which reduces cytochrome *c* and pumps protons across the IM in oxidative phosphorylation, and aconitase, another of the citric acid cycle enzymes. Fe/S clusters are synthesized exclusively in the matrix of the mitochondrion. The process of Fe/S cluster assembly is acutely sensitive to oxidative stress via O_2 or reactive oxygen species (ROS). The matrix is uniquely suited for this task as it is the most anaerobic compartment in a eukaryotic cell (16).

The synthesis of Fe/S clusters is a concerted process involving multiple proteins. While the proteins involved in this pathway have been identified, their precise roles are often not well understood. Fe^{2+} ions are imported into the matrix via the putative transporters Mrs3p, Mrs4p, Mmt1p and Mmt2p (17, 18). The proteins Nfu1p, Isa1p, Isa2p, Isu1p, and Isu2p serve as "scaffold proteins", so named because they contain structural elements that facilitate the assembly of nascent Fe/S clusters (19, 20, 21, 22). The resulting clusters are reduced through the adrenodoxin Yah1p (23, 24) and the adrenodoxin reductase Arh1p, which obtains reducing equivalents from NADH. At this point, nascent clusters bound for matrix and IMS apoproteins are inserted into their targeted proteins, possibly through transferase-like chaperones such as Bat1p (25). Clusters bound for extramitochondrial apoproteins must also be ferried through the matrix, again using a chaperone like Bat1p, and delivered to Atm1p, a transmembrane protein of the IMS. Atm1p shuttles clusters across the IMS, where they are transferred to the sulfhydryl oxidase Erv1p (26). Other matrix-localized proteins, such as Yfh1p and Jac1p, are essential to Fe/S cluster assembly but their precise roles remain unclear. The process by which newly synthesized Fe/S clusters are exported from the mitochondria is also unclear. Erv1p probably interacts with a transmembrane protein, possibly a TOM protein complex on the outer membrane. A similar family of protein complexes in archaea and prokarya, the Tat complexes, has demonstrated an ability to transport Fe/S clusters across membranes (27). Once the clusters are transported to the cytosol they are transferred to their target proteins, possibly by the aminotranferase protein Bat2p, a cytosolic homolog of the aforementioned matrix protein Bat1p (26).

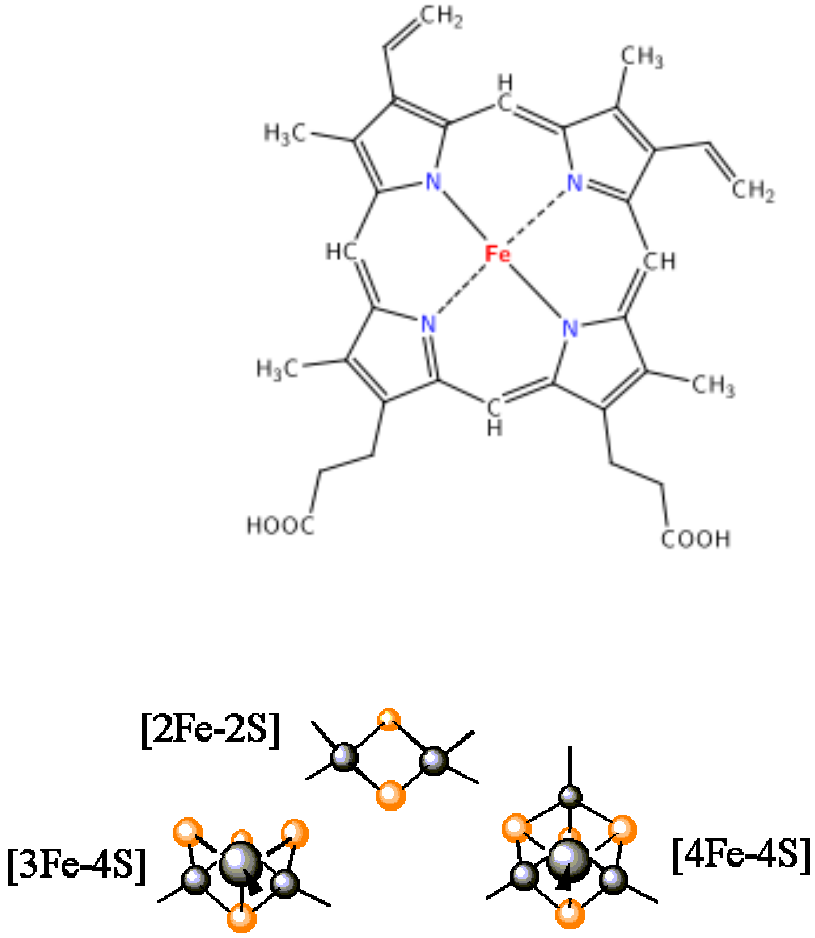

Figure 1-1. Examples of heme and Fe/S cluster cofactors. Shown are heme *b* (upper structure) and [2Fe-2S], [3Fe-4S], and [4Fe-4S] cofactors. For the Fe/S clusters shown above, Fe atoms are shown in gray and S atoms are shown in orange (taken from http://en.wikipedia.org).

In addition to iron, copper and manganese are essential transition metals in mitochondrial homeostasis. Cytochrome *c* oxidase requires two equivalents of copper for proper function, with both Cu_A and Cu_B operating as electron transfer agents in tandem with heme *a* and heme a_3, respectively. Cox23p, Cox17p, Sco1p, and Cox11p function as chaperones for the import and assimilation of copper ions into mitochondria and insert them into the cytochrome oxidase apoproteins Cox1p and Cox2p during their assembly (28, 29, 30). Copper ions in these chaperones are in the diamagnetic Cu^+ oxidation state. Manganese is found in the active site of the mitochondrially-localized superoxide dismutase, Sod2p. The chaperone protein Mtm1p imports manganese ions and coordinates the insertion of Mn^{2+} into the matrix-localized apo-Sod2p (31). Interestingly, the processes of iron and copper metabolism are intricately linked in yeast. The proteins Ctr1p, essential in copper transport across the cellular plasma membrane, and Fet3p, a blue multicopper oxidase, are required for iron uptake in *Saccharomyces cerevisiae* (32).

The protein complexes that carry out oxidative phosphorylation contain a great number of Fe/S clusters and heme cofactors. Complex II, alternatively known as succinate dehydrogenase, is an integral inner membrane protein containing three Fe/S clusters, a [2Fe-2S], [3Fe-4S], and [4Fe-4S] as well as a cytochrome *b* subunit. This protein complex generates $FADH_2$ from the oxidation of succinate to fumarate as part of the citric acid cycle, with the Fe/S clusters acting as a "molecular wire" to transfer electrons for the reduction of FAD. The resulting $FADH_2$ is then oxidized via reduction of ubiquinone (Q) to ubiquinol (QH_2).

QH_2 is oxidized back to Q by cytochrome bc_1, named for the heme-containing cytochromes in the complex. In addition to the hemes b_L and b_H found in cytochrome *b* and heme c_1 in cytochrome c_1, the protein complex also contains a [2Fe-2S] cluster commonly referred to as the "Rieske" center. The heme and Fe/S cluster centers couple electron transfer from Q to another heme-containing protein, cytochrome *c*, through a process known as "the Q cycle". Two electrons are abstracted from a Q in the Q_o site, with one transferred to the Rieske center, followed by cytochrome c_1, and finally to cytochrome *c*, which vacates the protein complex with concomitant release of Q from the Q_o site. The second electron is transferred to cytochrome b_L and then to cytochrome b_H, where it reduces a Q bound in the Q_i site to a radical, semiquinone state. The process is repeated, with a new QH_2 molecule bound in the Q_o site and the reduction of a second equivalent of cytochrome *c* and reduction of the semiquinone radical to QH_2.

Reduced cytochrome *c* transfers an electron to the Cu_A site of the protein complex cytochrome *c* oxidase. This site transfers the electron to heme *a*, which subsequently transfers the electron to heme a_3, and finally to Cu_B. The process is repeated, only this time heme a_3 is the terminal electron acceptor. Heme a_3 then binds a molecule of O_2 and forms a Fe-O-O-Cu peroxo bridge with Cu_B. A third reducing equivalent from cytochrome *c* is introduced with a proton, resulting in a ferryl (Fe^{4+}=O) moiety and a Cu^{2+}-OH. A fourth reducing equivalent from cytochrome *c* reduces the ferryl to a ferric Fe^{3+}-OH group. Two additional protons are then coordinated, one each at the Fe^{3+}-OH and Cu^{2+}-OH sites, and two molecules of water are released. The protons used in reducing O_2 to water in this process are removed from the matrix, contributing to

the proton gradient. Additionally, four uncoordinated protons are pumped across the inner membrane during this process, resulting in eight protons being removed from the matrix. The free energy resulting from the proton gradient is coupled to the synthesis of ATP, an endergonic process (33).

The example of oxidative phosphorylation, with a myriad of proteins, cofactors, and substrates reacting in a concerted manner, illustrates the inherent complexity found in many biological systems. Systems biology is a discipline that seeks to integrate different levels of information to understand how a biological system works. The relationships and interactions between various parts of a biological system are studied with the goal attaining a molecular-level understanding of the whole system. Systems biology, in which a complex biological entity or process is evaluated as a whole, is by no means a contemporary concept. The work of Descartes (34) and others developed the idea of "scientific reductionism". This idea seeks to simplify complex problems or systems into their representative components and argues, for example, organisms can be described in terms of their DNA, while DNA can be described in terms of the atoms comprising it, and so forth. Indeed, systems biology faithfully follows this line of reasoning in that a biological system, e.g. a cell, is taken as a whole and described as a function of the various metabolic and reproductive processes and reactions required to sustain it. Systems biology can be viewed hierarchically as complex processes or behaviors at a higher level and the molecular events that give rise to those processes at a lower level. A systems biological analysis will explain the complex process or behavior using known molecular-level interactions. A broad example lies in the development of

proteomics, genomics, metabolomics, and other "-omics" strategies. These techniques provide researchers with the necessary tools to investigate systems biology problems, for example, describing metabolic processes in an organism or cell. In relation to this work, one can view Fe/S cluster metabolism as a complex system arising from the import of nascent Fe ions, the abstraction of sulfur from cysteine, the synthesis of nascent Fe/S clusters, the export of clusters to their apoproteins, and so forth. These processes could be further reduced to the individual molecular events that comprise each of the aforementioned steps. One setback in using this approach is drawing relevant scientific conclusions from the often intractable amounts of data obtained from these system-wide studies. As with proteomics or genomics, the investigation of the events and components involved in the assimilation of transition metal ions in mitochondria, hence, a mitochondrial "metallo-omics" analysis, may yield insights into transition metal metabolism in these organelles. The ability to distinguish and quantitate the various transition metal environments at the molecular level in a biological system as complex as a mitochondrion is a challenge that has not been addressed. The problem is the absence of appropriate techniques that would allow molecular-level resolution on complex samples, in analogy to the use of microarrays in studying individual mRNA transcripts present in a cell. This dissertation explores whether the use of electronic paramagnetic resonance (EPR) and Mössbauer spectroscopies, supported with protein and transition metal quantitation, is sufficient to resolve individual Fe environments within mitochondria, and thus allow molecular level insights into complex Fe-associated processes occurring within the organelle.

EPR is useful in studying entities with unpaired electrons. This spectroscopy uses microwave radiation to probe the electronic structure of paramagnetic species, from which information regarding the redox state and coordination environment of an EPR active center can be obtained. An experiment can be performed at temperatures ranging from room temperature down to 4 K or lower, depending on the instrumental setup. Spectra are normally obtained for half-integer spin systems, i.e., $S = 1/2, 3/2$, etc., while integer spin systems, such as $S = 1, 2$, etc., are often "EPR silent" due to large zero-field splittings (35). For the transition metals Fe, Cu, and Mn, the valence states most easily observed in EPR experiments are high- and low-spin Fe^{3+}, Cu^{2+}, and Mn^{2+} systems, respectively.

EPR has been used to study mitochondrial metalloproteins and membranes as well as cofactors containing organic radicals. The presence of Mn^{2+} and their effect on the homeostasis of mammalian mitochondria has been reported (36). The Cu_A site in cytochrome oxidase from ox heart mitochondria has been investigated via EPR to determine orientational and spatial information regarding the protein's active site (37). The [2Fe-2S] Rieske center in cytochrome bc_1 has been extensively studied by EPR (38, 39). The electronic properties of the heme and Fe/S clusters of succinate dehydrogenase have been investigated (40, 41). EPR has been used to investigate the effects of reactive oxygen on mitochondrial membranes (42) and membrane bound proteins and lipids (43). Whole mitochondria isolated from rat heart have been analyzed via EPR to determine the extent of damage to EPR active centers in the respiratory chain during ischemia (44).

Flavins and ubiquinone can be stabilized in an $S = 1/2$ semiquinone state that affords an EPR signal at the free-electron g-value, 2.00. Flavin-containing mitochondrial proteins include α-ketoglutarate dehydrogenase (45), *D*-lactate cytochrome *c* oxidoreductases (46), glutathione reductase (47), thioredoxin reductase (48), glycerol-3-phosphate dehydrogenase (49), *D*-arabino-1,4,-lactone oxidase (50), acetolactate synthase (51), methylene tetrahyhdrofolate reductase (52), succinate dehydrogenase (53), Coq6p (54), and Mmf1p (55).

Like EPR, Mössbauer spectroscopy has been used to investigate iron-containing centers in mitochondria. Iron accumulation in rat liver mitochondria has been reported (56). A single type of iron center was identified that exhibited properties consistent with adventitiously associated, high-spin Fe^{3+} and likely not incorporated in the active site of any iron-containing proteins. The human homolog of yeast Nfu1p has been characterized for its ability to assemble nascent Fe/S clusters (57). A recent study investigated the [2Fe-2S] center in human Grx2, a glutathione-dependent oxidoreductase involved in redox homeostasis under conditions of oxidative stress (58). Whole mitochondria from yeast have been previously analyzed by Mössbauer spectroscopy (59). The spectra reported contained no discernable signals in spectra obtained from unaltered, wild-type mitochondria.

The work comprising this dissertation seeks to provide foundational information regarding the identification and quantitation of EPR- and Mössbauer-active metal centers in intact mitochondria from the model organism *Saccharomyces cerevisiae* using a systems biology approach. As mentioned, previous studies focused primarily on the

spectroscopic characterization of *individual* proteins, cofactors, or membranes, or possibly individual proteins, membranes, or cofactors in intact mitochondria. These previous studies provided valuable information in their own right, however, these study did not address the global distribution of Fe centers in this organelle. One problem was that signal/noise ratios were quite low such that many signals could have been missed. Thus, this problem must be addressed before intact mitochondria could be studied by EPR and Mössbauer spectroscopies. Another challenge in performing such a study lies in the potentially large number of contributing centers in the spectra of intact mitochondria. Thus, another issue explored in this discertation was the degree to which these two biophysical methods, in conjunction with analytical characterization, could resolve the Fe-containing species in mitohcondria. The results of this study suggest that these biophysical methods can afford *partial* resolution into *groups* of Fe-containing proteins. Nevertheless, the analysis afforded new and substantial insights into the distribution and composition of Fe-containing species within mitochondria, a cellular organelle of extreme complexity.

CHAPTER II

METHODOLOGY AND PROTOCOLS

Materials

All reagents and chemicals, unless other noted, were purchased from Fisher Scientific, Sigma Aldrich, or Gold Biotechnology. ^{57}Fe was purchased from Cambridge Isotope Laboratories. Atomic absorption spectroscopy standard solutions were purchased from Environmental Express. Ar, N_2, O_2, CO, and air gas cylinders were purchased from Praxair through the Texas A&M University Department of Chemistry Stockroom. *Saccharomyces cerevisiae* strain D273-10B was purchased from American Type Culture Collection.

Growth of Saccharomyces cerevisiae

The following protocol describes the growth of *Saccharomyces cerevisiae*. It is modified from a previously reported protocol (60). The protocol was scaled up from the previously reported protocol for 24 liters of growth media, which is inoculated with 1 liter of D273-10B grown to an optical density at 600 nm of 1.2 to 1.4. The following components comprised the 24 liter growth media:

1. 72 g yeast extract
2. 24 g NH_4Cl
3. 24 g KH_2PO_4
4. 12 g NaCl
5. 12 g $CaCl_2 \cdot 2H_2O$

6. 14.4 g $MgCl_2 \bullet 6H_2O$

7. 12 g glucose

8. 500 mL Na^+(lactate)

Procedure

The media was distributed among four 9 liter Kimax™ media bottles, capped with rubber stoppers containing both a glass transfer rod (8 mm outer diameter, 50 cm long) and an additional glass rod (4 mm outer diameter, 10 cm long) for air flow during transfer of the media. The bottles had their glass tubes capped with aluminum foil and were autoclaved at 121º C with 20 minutes total exposure time. The media was then removed from the autoclave and transferred to a cold room operating at 4º C for cooling. During this cooling period a jacketed, 25 liter bioreactor outfitted with a large glass transfer rod and a fritted gas dispersion rod, a two meter section of Tygon® tubing (8 mm outer diameter), and a 20 cm long plastic tube stuffed with cotton wadding and connected to a 15 cm section of Tygon® tubing (4 mm outer diameter) was cleaned using DD-H_2O and autoclaved at 121º C for 20 minutes total exposure time. The bioreactor was then transferred to a cold room operating at 4º C for cooling.

When both the media and bioreactor had reached room temperature, the bioreactor jacket was connected to a water circulator and filled with water. The water circulator was set to operate at 30º C. The media was then transferred into the bioreactor by connecting the larger glass rod in the cap of a media bottle to the autoclaved, two meter section of Tygon® tubing while the smaller glass rod was connected to the plastic tube stuffed with cotton wadding to prevent airborne contaminants from entering the

bioreactor during media transfer. The two-meter Tygon® tubing was connected to a large glass rod on the lid of the bioreactor while clamped to a peristaltic pump. The pump was turned on and the contents of the media bottle were completely emptied into the bioreactor. This process was repeated for the remaining three media bottles. Following media transfer, the transfer tube on the bioreactor was capped with aluminum foil. A separate Tygon® tube connected to an O_2 gas cylinder was then connected to the fritted gas rod on the bioreactor and O_2 was bubbled at a rate of 6 liters per minute. At this point the one-liter yeast culture was poured into the bioreactor and allowed to grow until it reached an optical density at 600 nm of 1.2 to 1.4. A typical yield resulted in a cell paste of 100 to 150 g.

For the Mössbauer experiments described in this work, cells were grown as described above, however, the 24 liter growth media was supplemented with 20 μM $^{57}FeCl_3$.

Purification of mitochondria from Saccharomyces cerevisiae

The following protocol describes the isolation of crude mitochondria from *Saccharomyces* cerevisiae. It is modified from a previously protocol (60). From a cell paste of 100-150 g, the typical yield is 150-200 mg mitochondrial protein. The method can be up- or downscaled by a least a factor of two. The procedure requires the following isolation buffers:

1. Buffer TD: 100 m*M* Tris-SO_4. pH 9.4, 10 m*M* DTT; prepare fresh before use (350 ml)

2. Buffer SP: 1.2 *M* sorbitol, 20 m*M* potassium phosphate, pH 7.4 (1000 ml)
3. Buffer 2 × SHP: 1.2 *M* sorbitol, 40 m*M* HEPES-KOH, pH 7.4 (200 ml)
4. DD-H_2O + PMSF (phenylmethylsulfonyl fluoride) (200 ml)
5. Buffer 1 × SH: 0.6 *M* sorbitol, 20 m*M* HEPES-KOH, pH 7.4 (200 ml)
6. Buffer 2 × SH: 1.2 *M* sorbitol, 40 m*M* HEPES-KOH, pH 7.4 (200 ml)

Unless otherwise indicated, all manipulations were carried out in an anaerobic glove refrigerated to 5º C. All buffers were degassed using a Schlenk line prior to transfer into the anaerobic glove box.

Procedure

1. Cells were spun by centrifugation for 5 minutes at 5000 rpm at room temperature in tared bottles using a Sorvall SLC-6000 fixed-angle rotor in a Sorvall Evolution fixed-angle centrifuge.
2. Cells were then resuspended in 200 mL H_2O and spun by centrifugation for 5 minutes at 5000 rpm using a Sorvall SLC-6000 fixed-angle rotor in a Sorvall Evolution fixed-angle centrifuge. The supernatant was poured off and the wet weight of the cells was determined.
3. The yeast lytic enzyme Zymolyase 100T, with a lytic activity of 100 000 units per gram, was added to 25 mL buffer SP. 1.5 mg of enzyme were added per gram of cells. The activity of the Zymolyase 100T enzyme will be higher when it is solvated at this point in the procedure versus waiting until step 6 (where it is added to the cells) to dissolve it.

4. Cells were then resuspended in 500 mL buffer TD using a rubber policeman and incubated for 15 minutes at 30° C with gentle shaking.
5. Cells were spun by centrifugation for 5 minutes at 5000 rpm at room temperature using a Sorvall SLC-6000 fixed-angle rotor in a Sorvall Evolution fixed-angle centrifuge and the pellet was resuspended in 250 mL buffer SP.
6. Step 5 was repeated and the Zymolyase solution was added.
7. The cell/Zymolyase solution was incubated at 30° C for one hour with gentle shaking (150 rpm).
8. All subsequent operations were conducted at 5° C. Spheroplasts were collected through spinning by centrifugation at 5000 rpm for 5 minutes using a Sorvall SLC-6000 fixed-angle rotor in a Sorvall Evolution fixed-angle centrifuge.
9. The resulting pellet was carefully suspended in 250 mL ice-cold buffer SP with a rubber policeman and the spheroplasts were spun by centrifugation at 5000 rpm for 5 minutes using a Sorvall SLC-6000 fixed-angle rotor in a Sorvall Evolution fixed-angle centrifuge. This step was repeated once.
10. The spheroplasts were then resuspended in 200 mL buffer 2 × SHP. The final volume was measured and the spheroplast solution was diluted with one volume (200 mL plus the volume of the spheroplasts) of ice-cold H_2O containing 1 m*M* PMSF.
11. The resulting suspension was homogenized in a 50 mL glass homogenizer with a glass piston using 20 strokes and poured into four 250 mL centrifuge bottles.

12. The bottles were spun by centrifugation twice at 2500 rpm for 5 minutes using a Sorvall SLC-1500 rotor in a Sorvall Evolution fixed-angle centrifuge. Following each spinning the centrifugation bottle was returned to the glove box and the supernatant was poured into a 250 mL centrifuge tube.
13. The tube was centrifuged by spinning at 10 000 rpm for 10 minutes using a Sorvall SLC-1500 rotor in a Sorvall Evolution fixed-angle centrifuge. The resulting supernatant was removed and discarded.
14. The pellet, comprised of mitochondria, was resuspended in 5 mL of buffer 1 × SH using a 1 mL pipetman. The resulting suspension was further diluted with 50-100 additional mL of buffer 1 × SH.
15. The solution is spun by centrifugation at 2500 rpm for 5 minutes using a Sorvall SLC-1500 rotor in a Sorvall Evolution fixed-angle centrifuge. The supernatant is poured into two fresh 38 mL Beckman Ultra-Clear™ ultracentrifuge tubes and spun by centrifugation at 10 000 rpm for 10 minutes using a Beckman SW-32Ti rotor in a Beckman L7 ultracentrifuge.
16. The resulting pellet was resuspended in 5 mL of Buffer 1 × SH using a 1 mL pipetman. The pellet was broken up by gently drawing it up into the tip of the pipetman and expelling it.

The following protocol is used to set up a discontinuous Nycodenz® gradient in order to purify the crude mitochondrial fraction and yield “high purity mitochondria”, i.e. a mitochondrial fraction devoid of unbroken yeast cells as well as translational organelles such as the endoplasmic reticulum and the Golgi apparatus. A typical cell

harvest requires between two and four of these gradients, each of which is prepared in 25 mm × 89 mm Beckman Ultra-Clear™ ultracentrifuge tubes. These tubes were placed in the buckets of a Beckman SW-32Ti swinging bucket rotor. The protocol is modified from a previously reported protocol. The following reagents and buffers are required for the purification:

1. Buffer 1 × SH: 0.6 M sorbitol, 20 mM HEPES-KOH, pH 7.4
2. Buffer 2 × SH: 1.2 M sorbitol, 40 mM HEPES-KOH, pH 7.4
3. 20% Nycodenz: For 10 mL mix 6 mL buffer 2 × SH with 4 mL 50% Nycodenz solution
4. 15% Nycodenz: For 10 mL mix 7 mL buffer 2 × SH with 3 mL 50% Nycodenz solution

Procedure

1. All steps were conducted in an anaerobic glove refrigerated to 5º C. 50 mg of mitochondrial protein was loaded on the 10-mL Nycodenz gradient on step 2.
2. The Nycodenz density step gradients were prepared in 25 × 89-mm Ultra-Clear centrifuge tubes suitable for the Beckman SW-32Ti rotor. Gradients were formed just before use by overlaying 5 mL of 25% (w/v) Nycodenz solution with 5 mL of 15% (w/v) Nycodenz solution.
3. The step gradient was overlaid with a solution of freshly isolated mitochondria (in 1 mL buffer 1 × SH) obtained from previous procedure.

4. The tubes were centrifuged by spinning at 20 000 rpm for 2 hours in a Beckman SW-32Ti rotor using a Beckman L7 ultracentrifuge. Purified mitochondria appeared as a brownish band at the 15%/25% gradient interface.
5. The solution was removed by aspiration and purified mitochondria were harvested with a 1 mL pipetman. The sample was then diluted with 5-10 mL of buffer 1 × SH. This solution was centrifuged for 10 minutes at 10 000 rpm in a Beckman SW-32Ti swinging-bucket rotor using a Beckman L7 ultracentrifuge.
6. The supernatant was poured off and the resulting pellet was resuspended in 2 ml of buffer 1 × SH using a 1 mL pipetman. The pellet was broken up by gently drawing it up into the tip of the pipetman and expelling it. The pellet was resuspended and transferred to a 15 mL Falcon tube.

Preparation of samples for electron paramagnetic resonance (EPR)

Custom-built Delrin™ inserts were designed to fit within the buckets of the SW-32Ti rotor. Holes were drilled into the center of these inserts, with a diameter just sufficient to fit a modified EPR tube (5 mm OD; 3.2 mm ID; 87.6 mm long; Wilmad/Lab Glass, Buena NJ) and a 2 mm-high cylinder of silicone rubber which was placed at the bottom of the Delrin™ insert shown if Figure 2-1. The brown mitochondrial solution (1-2 mL)

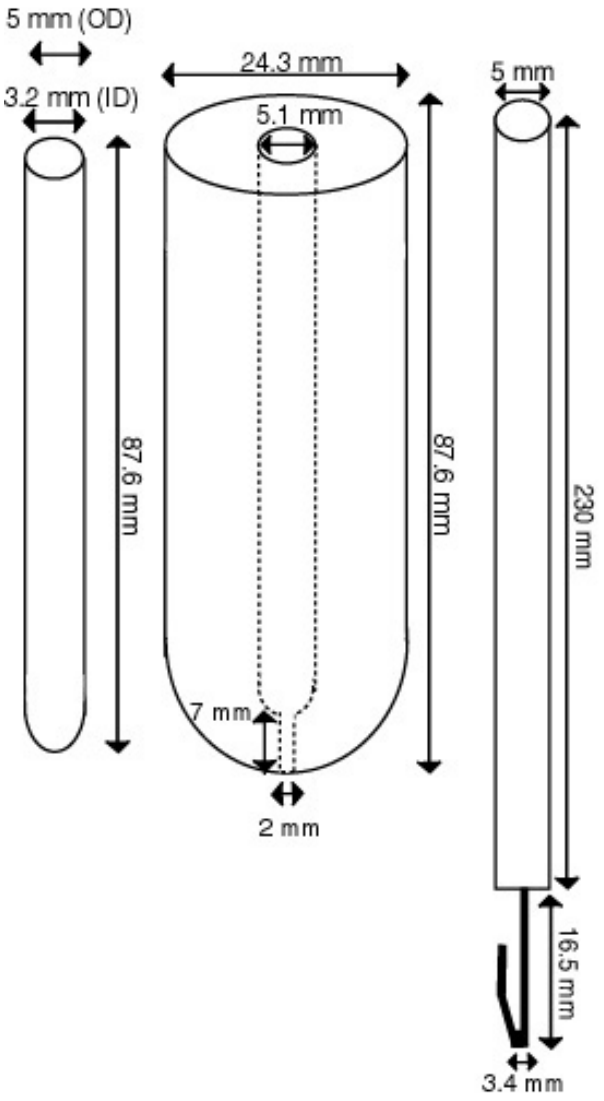

Figure 2-1. Equipment developed for maximizing the signal-to-noise ratio of mitochondrial EPR samples. Shown are a modified EPR tube (left), Delrin™ insert (center), and EPR tube appendage (right).

obtained from the gradient step described above was diluted to 5 mL with *SH* buffer. Tubes were filled with this solution and the entire assembly was sealed, removed from the box, spun by centrifugation at 7000 rpm for 4 hr, and then returned to the box. The supernatant was replaced with additional mitochondrial solution. This process was repeated until the volume of tightly packed mitochondria at the bottom of the tube reached ca. 400 μL. Two to four EPR samples were prepared from a solution of gradient-purified mitochondria isolated from 25 L of culture. EPR tubes were removed from the inserts and frozen in 20 sec using liquid N_2.

A thin (1 mm) quartz rod was bent into the shape of a "J" (40 mm long-end, 20 mm short-end and 4 mm width) and the long end was attached to the bottom of a standard EPR tube. The short end of the "J"-shaped rod was of a resiliency such that it could be inserted, when compressed gingerly, into the top of a mitochondria-containing EPR tube. The entire assembly (Figure 2.1) was sufficiently robust to be inserted into and removed from the EPR cavity.

EPR data collection and analysis

Spectra were obtained with a Bruker EMX X-band EPR spectrometer operating in perpendicular mode with an Oxford Instruments EM910 cryostat. Signals were simulated using either the program QPOWA (61) or software written by Michael P. Hendrich (Carnegie Mellon University). Parameters for each simulation described in this dissertation are provided in Appendix I. Signal intensities were quantified relative to a

Cu(II)EDTA spin standard. These intensities were obtained using the previously reported formula (62) given in the following equation:

$$SI = N \cdot \frac{1}{g_{ave}} \cdot SW^2 \cdot \frac{1}{\sqrt{P}} \cdot \frac{1}{T} \cdot \frac{1}{MA} \cdot \frac{1}{G}$$

where: SI = signal intensity
N = second integral of signal
g_{ave} = average g value for the signal
SW = sweep width
P = microwave power
T = temperature in Kelvins
MA = modulation amplitude
G = receiver gain

The resulting data were transferred into OriginLab® Version 7.5 (OriginLab Corp., Northampton, MA) for spectral analysis and signal quantitation.

Mössbauer spectroscopy

Custom-built Delrin™ inserts were designed to fit within the buckets of the SW-32Ti rotor. Holes were drilled into the center of these inserts, with a diameter just sufficient to fit a Mössbauer sample cup (12.1 mm OD; 10.9 mm ID; 9.60 mm long) and a 2 mm-high cylinder of silicone rubber which was placed at the bottom. The brown mitochondrial solution (1-2 mL) obtained from the gradient step described above was diluted to 5 mL with SH buffer. The insert/cup construction was filled with this solution and the entire assembly was sealed, removed from the box, spun by centrifugation at 9000 rpm for 2 hours, and then returned to the box. The supernatant was replaced with

additional mitochondrial solution. This process was repeated until the volume of tightly packed mitochondria at the bottom of the tube reached approximately 400 μL. One to three Mössbauer samples were prepared from a solution of gradient-purified mitochondria isolated from 25 L of culture. Mössbauer cups were removed from the inserts and frozen in 20 seconds using liquid N_2. Samples were run on two Mössbauer spectrometers using Janis Research Super-Varitemp Dewars, which allowed for studies in applied magnetic fields up to 8 T in the temperature range of 1.5 to 200 K. Mössbauer spectral simulations were performed using the WMOSS software package (WEB Research, Edina, MN). Isomer shifts are given in reference to iron metal at 298 K.

Determination of metal, protein concentrations

After spectra were obtained, a line was drawn on the exterior of the EPR tubes to indicate the height of the packed mitochondria. The contents were thawed and quantitatively transferred into a plastic screw-top vial using a slightly twisted quartz rod and a minimal volume of *SH* buffer. The volume of the packed organelles was determined by weighing the tube, before and after filling it with an equivalent volume of water, and dividing the difference by 0.997 g/mL. The final volume of the solution in the screw-top vial was similarly determined, typically 5 mL. The ratio of these two volumes constituted the dilution factor by which measured protein and metal concentrations, obtained using the solution in the vial, were multiplied to yield the respective concentrations in packed mitochondria.

Samples from the vial were sonicated using a Branson Sonifier 450 operating for 10 min at 60% capacity. Protein concentration was determined by quantitative amino acid analysis of aliquots that had been hydrolyzed in 6 *M* HCl/2% phenol at 110°C. The amino acid percentages were similar among all preparations (Supplemental material). All samples were analyzed using a Hewlett Packard AminoQuant system. Primary and secondary amino acids present in the samples were derivatized using *o*-phtalaldehyde and 9-fluoromethylchloroformate, respectively.

Iron, copper, and manganese concentrations were determined by atomic absorption spectrometry. Sonicated samples (250-400 μL) were digested using an equal volume of 15.8 M trace-metal grade HNO_3 (Fischer Scientific) in a sealed plastic tube that was then incubated overnight at 50°C. The resulting solution was diluted with deionized and distilled H_2O to a final HNO_3 concentration of 0.2 *M*. Metal concentrations were determined using a Perkin-Elmer AAnalyst 700 atomic absorption spectrophotometer operating in furnace mode. Standards for Fe, Cu, and Mn were prepared from commercially available standards containing a concentration of 1 mg/mL of the analyte of interest in 2% HNO_3. Standards of 0.10, 0.25, 0.50. 0.75, 1.0, 1.5, 2.0. and 2.5 μM concentrations were prepared using the aforementioned standard solutions and 0.2 M HNO_3 for Fe, Cu, and Mn. A volume of 600 μL for each standard solution was injected into a fresh sample cup, along with a 0.2 M HNO_3 acid blank, and placed in the spectrometer's autosampler. The signal area of the acid blank was subtracted from the signal area of the standards. The slit width was set at 0.2 mm for Fe and Mn and 0.7 mm for Cu. The lamp current was 30 mA for the Fe lamp, 15 mA for the Cu lamp, and

20 mA for the Mn lamp. The slope was 1.0 for the Fe standard calibration curve, 1.2 for the Cu standard calibration curve and 1.0 for the Mn calibration curve.

Electron and fluorescence microscopy

One mL of the resulting brown solution was spun by centrifugation in a Fisher Scientific microcentrifuge at 6400 rpm for 5 min in a 1.5 mL Eppendorf tube. The pellet was resuspended in *SH* buffer and glutaraldehyde (2.5% v/v final concentration) was added. The solution was recentrifuged and the pellet was resuspended in 1% osmium tetroxide and 0.5% potassium ferricyanide (w/v) in *SH* buffer. This was followed by *en bloc* staining using 1% uranyl acetate in *SH* buffer. Samples were dehydrated by incubation in increasingly concentrated ethanol solutions and then embedded using epoxy-based resin. Thin-sectioning was performed using a glass knife/water trough on a microtome, followed by retrieval of the thin sections using 200 mesh grids. Positive staining of these sections was performed using lead acetate/sodium hydroxide (63). Images were obtained using a JEOL 1200 EX TEM.

For fluorescence images, equivalent mitochondrial solutions were incubated in 0.6 *M* sorbitol/20 *mM* HEPES pH 7.4, containing 500 nM Mito Tracker® (Molecular Probes) or, in another experiment, 1 μM ER Tracker™ at 37° C for 45 min. The solution was centrifuged, and the pellet was resuspended in SH buffer. Images were obtained using a BioRad Radiance 2000 MP equipped with a 63X (water immersion) objective.

CHAPTER III

ELECTRON PARAMAGNETIC RESONANCE OF INTACT MITOCHONDRIA

Fifteen independent preparations of intact yeast mitochondria were isolated as described in Chapter II. Preparations *A1 – A4* were isolated without adding a metal chelator to the isolation buffers, preparations *D1 – D3* were isolated with EDTA (ethylenediaminetetraacetic acid) in all isolation buffers, and preparations *G1 – G8* were isolated with EGTA (ethylenebis(oxyethylenenitrilo)tetraacetic acid) (Acros) added to all buffers. These chelators were added to remove adventitious metal ions associated with mitochondria. EGTA is unable to penetrate biological membranes (64), while this property is uncertain with respect to EDTA. However, EDTA is commonly used in isolating mitochondria (65) and as far as we are aware, there have been no reports that EDTA strips essential metal ions from these organelles.

The isolation method was performed anaerobically essentially in the absence of oxidants and reductants. The only reductant used was DTT and then only at an early step of the isolation procedure. $E^{\circ'}$ for the disulfide/DTT half-cell is -330 mV versus NHE (66). Anaerobically-prepared isolation buffers almost certainly contain a trace of oxidizing ability (67).

Characterizing the purity, integrity, activity and composition of mitochondria is far more difficult than doing so for a single enzyme. Our approach was to use methods previously demonstrated to give rise to high purity mitochondria and to characterize

them multidimensionally. First, we assayed preparations for purity and membrane-integrity using electron microscopy. Although significant size dispersion was evident (Figure 3-1, upper panel), there was no obvious evidence of impurities or disrupted membrane structures. Sample morphology was independent of the method of isolation (as-isolated, EDTA- or EGTA-treated). Our images are similar to those obtained by the classical studies of Hackenbrock (68). Dispersion may result from the dynamic fission and fusion processes that are known to occur in yeast mitochondria (69). Confocal microscopic images reveal that mitochondria form extensive tube-like networks extending throughout the cell (70). These dynamic changes in size and shape render the concept of the *number* of mitochondria per cell rather meaningless. A more quantifiable parameter is the *volume* occupied by these organelles, and we will us this parameter throughout this dissertation.

Fluorescence microscopy of these samples also was used to assess purity. Samples used for fluorescence were stained with MitoTracker® and alternatively with Isolated mitochondria were tightly packed into custom-designed EPR tubes, using the low-speed centrifugation method described in *Experimental Procedures*. This maximized the concentration of mitochondria to afford EPR signals with the highest possible intensity by expelling external water. After spectra were obtained, samples were thawed and quantitatively transferred to another vial. Due to our concern that membrane integrity would be compromised by freeze/thaw cycles, EPR samples were never used twice (i.e. they were not thawed, treated in some manner, refrozen and reanalyzed

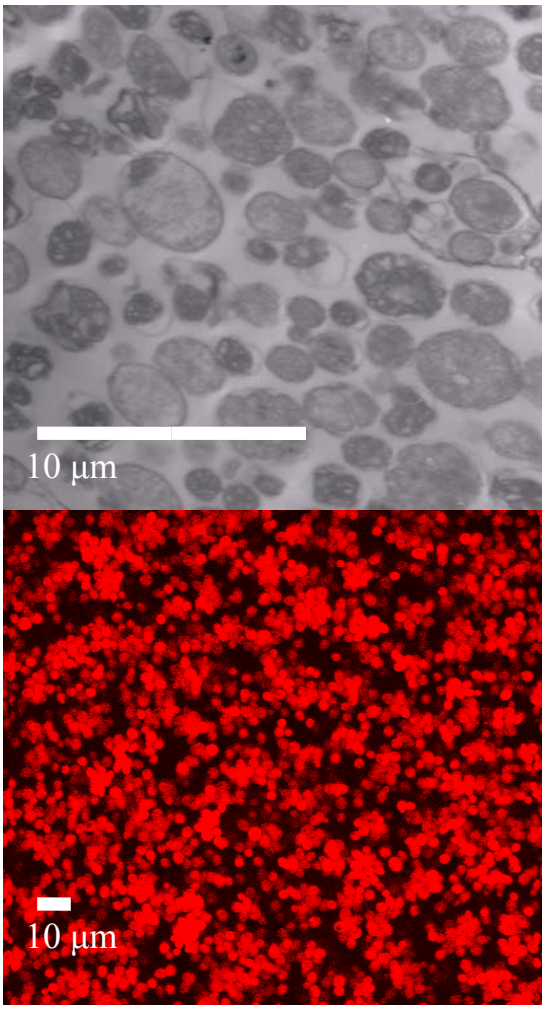

Figure 3-1. Electron (top) and fluorescence (bottom) microscopy images of whole mitochondria isolated from *Saccharomyces cerevisiae*.

Table 3-1. Protein and metal analysis of mitochondrial preparations.

Preparation	**Chelator**	**Protein (mg/ml)**	**[Fe] (μM)**	**[Cu] (μM)**	**[Mn] (μM)**
A1	none	38	570	260	30
A2	none	44	520	370	21
A3	none	44	640	390	24
D1	EDTA	83	780	430	12
D2	EDTA	48	590	390	13
D3	EDTA	52	600	320	14
G1	EGTA	42	540	340	14
G2	EGTA	52	570	310	14
G3	EGTA	43	510	270	15
Ave ± S.D.		50 ± 13	590 ± 82	340 ± 58	17 ± 6

EPR). Rather, thawed EPR samples were sacrificed for protein and metal analyses. We usedquantitative amino acid analysis to determine protein concentration, as this is the most accurate method available (71). Protein, iron, copper, and manganese concentrations are given in Table 3-1 for each preparation. If our tight-packing method excluded all exterior water, these values would reflect the concentrations of proteins and these metal ions in "neat" yeast mitochondria. In the more likely situation where some of the volume of our packed sampled was due to exterior water, the actual mitochondrial concentrations would be greater than those in Table 3-1. The corresponding averaged protein/metal ratios were 12 nmol Fe/mg protein, 6.8 nmol Cu/mg protein, 0.3 nmol Mn/mg protein.

EPR of as-isolated, intact mitochondria

The g = 6 and 2 regions of the EPR spectra of preparation *A1* are shown in Figures 3-2 and 3-3, respectively. Signals from five separate species can be identified. The signal at g = 4.3 is typical of high-spin (S = 5/2) nonheme Fe(III) species with E/D = 0.33. The signals at g = 6.8 and 5.0 are indicative of a high-spin heme Fe(III) species with E/D = 0.042. The signal at g = 6.0 appears to be from another high-spin heme Fe(III) species with E/D near 0. The six-line hyperfine pattern (A = 90 G) which dominates the g = 2 region is typical of a S = 5/2 Mn(II) species. A feature at $g \sim 1.94$ is also evident but is dominated by the hyperfine pattern (see next section). The region between g = 4.3 and 2.2 was devoid of signals. Quantification of the signals indicates [Mn^{2+}] = 20 μM, [Fe^{3+}, E/D = 0.33] = 40 μM, and [Fe^{3+}, E/D = 0.042] = 3 μM,

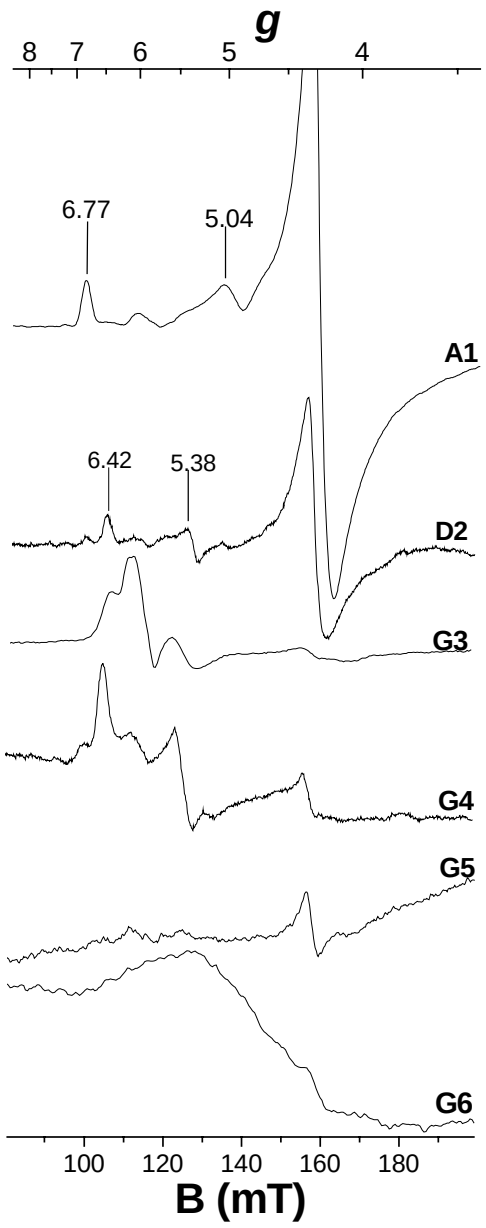

Figure 3-2. Low-field X-band EPR spectra of intact and redox treated mitochondrial preparations *A1*, *D2*, *G3, G4, G5* and *G6*. EPR conditions: microwave frequency, 9.429 (*A1*), 9.419 (*D2*), 9.478 (*G3*), 9.453 (*G4*), 9.468 (*G5*) and 9.458 (*G6*) GHz; microwave power, 20 mW; modulation amplitude, 10 G; receiver gain (*A1*, *D2*, *G3*), 1×10^4, (*G4*, *G5*, *G6*) 5.02×10^4; temperature, 10 K.

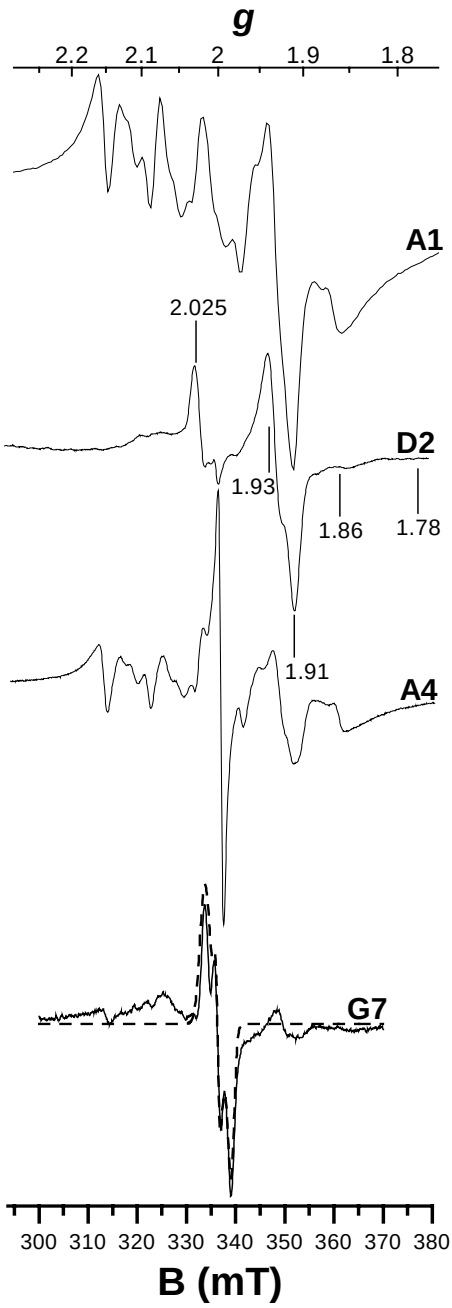

Figure 3-3. High-field X-band EPR spectra of intact and redox treated mitochondrial preparations *A1*, *D2*, *A4* and *G7*. Conditions were as in Figure 3-2 except that microwave frequency was 9.429 (*A1*), 9.424 (*D2* and *A4*) and 9.448 (*G7*) GHz.

Table 3-2. EPR signals observed from whole mitochondria from *Saccharomyces cerevisiae.*

Signal	*Spin State Parameters*	*g*-values (g_1, g_2, g_3)	Concentration Range (μM)	Tentative assignment
High-spin ferric heme 1	*S = 5/2, E/D = 0.042*	6.8, 5.0	0.3-3	Cytochrome *c* peroxidase (Ccp1p)
High-spin ferric heme 2	*S = 5/2, E/D =0.024*	6.4, 5.3	1-2	Cytochrome *c* oxidase (a_3:Cu_B)
High-spin ferric heme 3	*S = 5/2, E/D =0*	6.0	0.1-1	Cytochrome *c* oxidase (a_3:Cu_B)
g = 5.2	*S = 3/2*	5.22		$[4Fe\text{-}4S]^+$ clusters
g = 4.3	*S = 5/2, E/D =0.33*	4.27	20-40	Adventitious Fe^{3+}
g_{ave} = 2.34	*S = 1/2*	2.52, 2.34, 1.81	Minor	His-Fe-OH heme or cyt. P450-type center
g_{ave} = 2.15	*S = 1/2*	2.25, 2.20	Minor	Met-Fe-His heme
g_{ave} = 2.07	Spin-coupled system, *A* = 17 G	2.07, 2.01	10	Fe-NO heme
g_{ave} = 2.04	*S = 1/2* or spin-coupled system	2.085, 2.021, 2.007	1-9	Thiyl radical? Spin-interacting Fe/S cluster?
g_{ave} = 2.02	*S = 1/2*	2.026, 2.022, 2.003	0-5	Aconitase $[3Fe\text{-}4S]^+$ cluster
g = 2.00 (hyperfine)	*S = 5/2*; *I = 5/2*; *A* = 90 G	g_{ave} = 2.000	0-20	Adventitious Mn^{2+}
g = 2.00 (isotropic)	*S =1/2*	2.000, 2.000, 2.000	<0.2	C- or O-based organic radical
g_{ave} = 1.94	*S =1/2*	2.026, 1.934, 1.913	0-10	Succinate dehydrogenase $[2Fe\text{-}2S]^+$ (Sdh2p)
g_{ave} = 1.90	*S = 1/2*	2.025, 1.897, 1.784	10-20	Rieske $[2Fe\text{-}2S]^+$ cluster (Rip1p)

[Fe^{3+}, *E/D* = 0] = 0.1 μM. A compilation of signals and concentrations of species observed in this study is given in Table 3-2.

Given the complexity of mitochondria, it is important to consider reproducibility of spectral features. The same set of signals was observed in spectra from preparations *A2* and *A3*, with the intensities of the *g* = 1.94, *g* = 1.90, and the high-spin ferric heme signal tentatively assigned to Ccp1p fluctuating by no more than by a factor of two.

EPR of EDTA-treated intact mitochondria

Preparations *D1- D3* were obtained under the same as-isolated conditions just described, but with EDTA in the isolation buffers. The metal analysis indicates insignificant differences in protein, Fe, and Cu concentrations, relative to as-isolated samples, whereas the Mn concentration is perhaps slightly lower (Table 3-1). EPR spectra of preparation *D2* are shown in Figure 3-3 and 3-4. Again, the region between *g* = 4.3 and 2.2 was devoid of signals. The *g* = 4.3 signal again dominates the low-field region, but its intensity is approximately half that of the signal in spectra of as-isolated preparations. This suggests that all or most of this signal arises from adventitious Fe^{3+} a portion of which can be chelated by EDTA and might be loosely bound to mitochondria. The high-spin heme species with signals at *g* = 6.8, 5.0 (*E/D* = 0.042) is present, but its intensity has declined by a factor of 10, relative to spectra from as-isolated samples. On the other hand, new signals are evident at *g* = 6.4 and 5.3 which arise from a second high-spin heme species. Quantification of this species yields a spin concentration of 1 μM.

The Mn^{2+} species which dominated the high-field region of spectra from as-isolated samples is absent from the g = 2 region of EDTA-treated samples. This is consistent with the observed decline in Mn concentration (Table 3-1). The Mn^{2+} signal in the as-isolated sample is therefore likely to be an adventitious species, which is removed by chelation with EDTA. A major species in the g = 2 region of the spectra of the EDTA-treated samples has g = 2.026, 1.934, 1.913 (g_{ave} = 1.94). A second species is evident, with g = 2.025, 1.897, 1.784 (g_{ave} = 1.90). The g-values of both species are indicative of Fe/S proteins. Quantification indicates that both are present at ~10 μM in spectra of *D2*. A third species has a broad resonance at g ~ 2.08. Due to overlapping signals, it is difficult to give a clear description of this signal. However, as the temperature is raised (Figure 3-4), the g_{ave} = 1.94 and 1.90 signals broadened significantly at 130 K (Figure 3-4D), revealing a sharp isotropic signal at g = 2.00, and additional features which appear to be associated with the g ~ 2.08 resonance. A microwave power study at 10 K indicated that the g_{iso} = 2.00 signal is easily saturated at less than 1 μW. The other signals in the spectrum begin to saturate at powers greater than 80 μW. For the g_{ave} = 1.94 signal at 10 K, the microwave power which caused the {signal intensity divided by the square-root of power} to reach half of its maximum value was $P_{1/2}$ = 57 mW.

The spectrum of *D1* obtained at 10 K and 200 μW was decomposed by simulating various signals. As shown in the figure on p. 41, the simulated signals included the g_{ave} = 1.94 signal (B), the g_{ave} = 1.90 signal (C), and the g_{iso} = 2.00 signal (E). The simulation of the signal with the g ~ 2.08 resonance (D) was indicated from

the agreement of the overall sum of the four simulations overlaid on the data of Figure 3-5A. Thus, the high temperature spectrum (Figure 3-4D) and the simulated sum suggest that the other resonances associated with the g = 2.08 resonance are near g = 2.00 as shown. Spin quantification of the various signals gave the species concentrations listed in Table 3-2.

EPR of EGTA-treated intact mitochondria

Preparations *G1- G3* were obtained under the same as-isolated conditions just described but with EGTA rather than EDTA included in isolation buffers. Again, relative to as-isolated samples, there were no significant changes in protein, Fe, or Cu concentrations, but the concentration of Mn ions was again slightly lower (Table 3-1). EPR of EGTA-treated samples were somewhat more variable; the spectrum of *G1* (not shown) was similar to that of the EDTA treated samples while the spectrum of *G3* (Figures 3-3 and 3-4) has significant differences. The concentration of the heme species with *E/D* = 0.024 (g = 6.4, 5.3) has increased by a factor of two, while that of the heme species with *E/D* = 0.042 (g = 6.8, 5.0) is near zero. The concentration of the heme species with *E/D* ~ 0 (g = 6), which was very low in all other samples, is 1 μM in EGTA-treated samples. In the g = 2 region, a strong sharp signal with g_{ave} ~ 2.01 now dominates the spectrum. The g_{ave} = 1.90 signal is present at a concentration double of that observed in the EDTA-treated samples. The temperature dependence of the

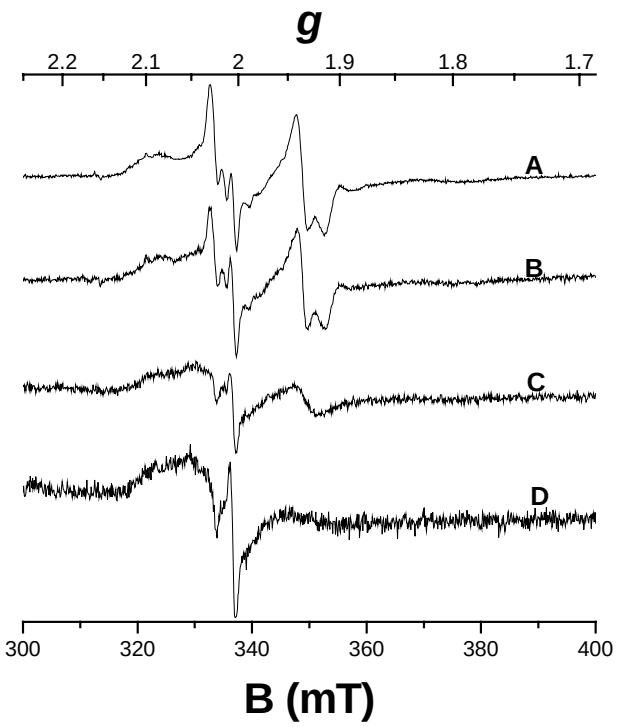

Figure 3-4. EPR temperature study of *D3*. (A), 20 K; (B), 40 K; (C), 50 K; (D), 130 K. Displayed intensities have been normalized by multiplying spectral intensities by the temperature at which they were collected.

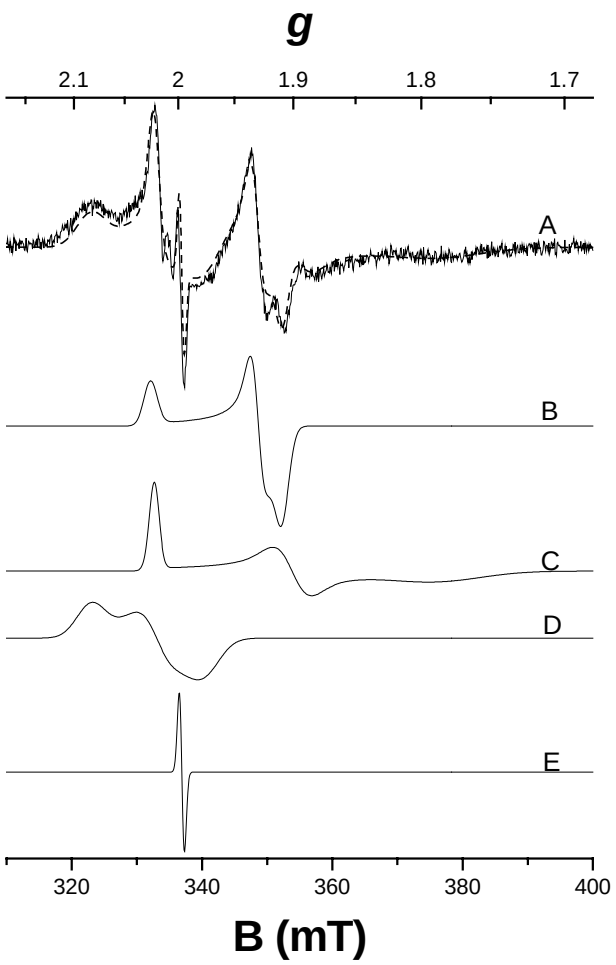

Figure 3-5. Simulations of the high-field region of the 10 K *D1* EPR spectrum. (A) Data (solid line) and combined simulation (dashed line); (B) $g_{ave} = 1.94$ signal; (C) $g_{ave} = 1.91$ signal; (D) $g_{ave} = 2.04$ signal; (E) $g_{ave} = 2.00$ signal. Conditions: microwave frequency, 9.414 GHz, microwave power, 20 μW, modulation amplitude, 10 G, receiver gain, 1×10^4.

G3 spectrum (Figure 3-6A-C) shows that the g_{ave} = 2.02 signal broaden significantly by 30 K, whereas the other signals are not affected. The microwave power dependence (Figure 3-6D-G) shows that this signal is strongly saturated at high powers relative to the other signals. The concentration of this species in *G3* is 5 μM.

Once these features of the g_{ave} = 2.02 signal were generally understood, we decomposed the high-field 10 K 2 μW spectrum of *G3* (Figure 3-7). Other signals simulated included those of Figure 3-6 as well as the g_{ave} = 2.02 signal. As was done for the spectral decomposition of the EDTA-treated sample, the intensity of each simulated signal was adjusted to produce a sum of simulations (Figure 3-7A) that matches the experimental spectrum. Simulation of the g_{ave} = 2.04 signal (Figure 3-7D) required slightly different values than was used for the simulation of Figure 3-5D, but the signals probably arise from the same species. Spin quantification of the various signals gave the species concentrations within the ranges listed in Table 3-2.

EPR of intact mitochondria in other redox and ligand-bound states

Other mitochondrial preparations were treated with various reagents in an effort to alter EPR features and afford additional insight into species that are present in these organelles. Prior to packing mitochondria into EPR tubes, we exposed samples to air for 24 – 48 hrs. We expected that the EPR spectrum of this sample (*A4*) would differ substantially from that observed in that of samples prepared entirely under anaerobic conditions. After repeated attempts, we resigned ourselves to the conclusion that, with one exception, differences with respect to spectra of as-isolated preparations were

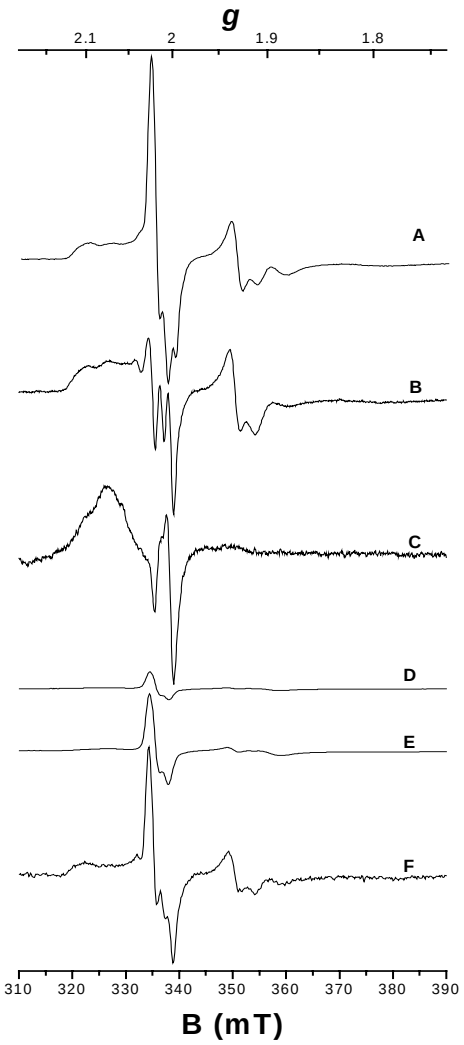

Figure 3-6. Temperature study (A through C) and power saturation study (D through F) of *G3*. For the temperature study at P = 20 mW: (A) T = 20 K; (B) T = 50 K; (C) T = 130 K. For the power study at T = 10 K: (D) P = 20 mW; (E) P = 2 μW; (F) P = 200 nW. Other conditions: microwave frequency, 9.478 GHz, modulation amplitude, 10 G, receiver gain, 1×10^4.

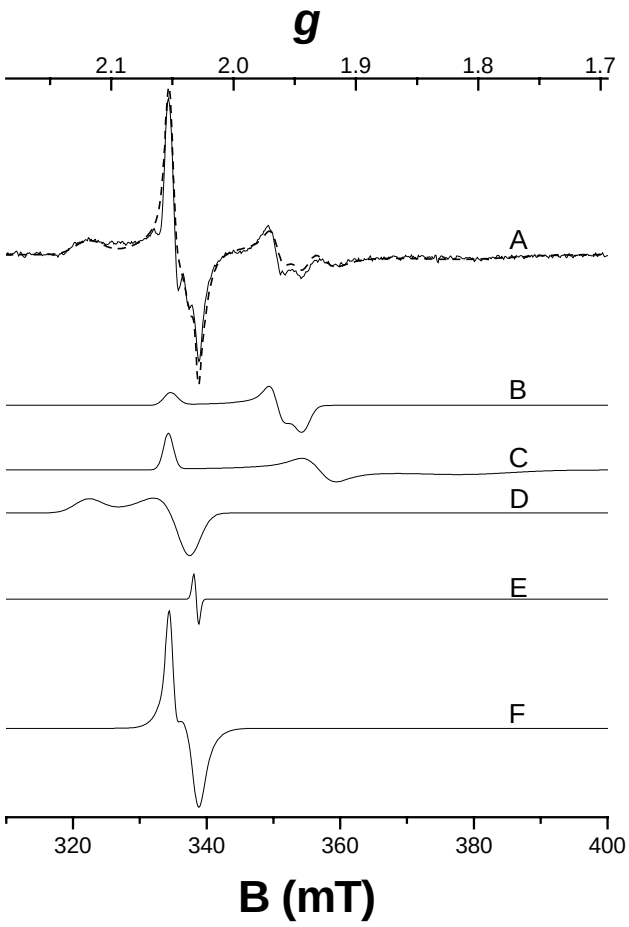

Figure 3-7. Simulations of the high-field 10 K EPR spectrum of *G3*. (A) Data (solid line) and composite simulation (dashed line), (B) $g_{ave} = 1.94$ signal; (C) $g_{ave} = 1.91$ signal; (D) $g_{ave} = 2.04$ signal; (E) $g_{ave} = 2.00$ signal; (F) $g_{ave} = 2.01$ signal. Other conditions: microwave frequency, 9.478 GHz, microwave power, 2 μW, modulation amplitude, 10 G, receiver gain, 5.02×10^4.

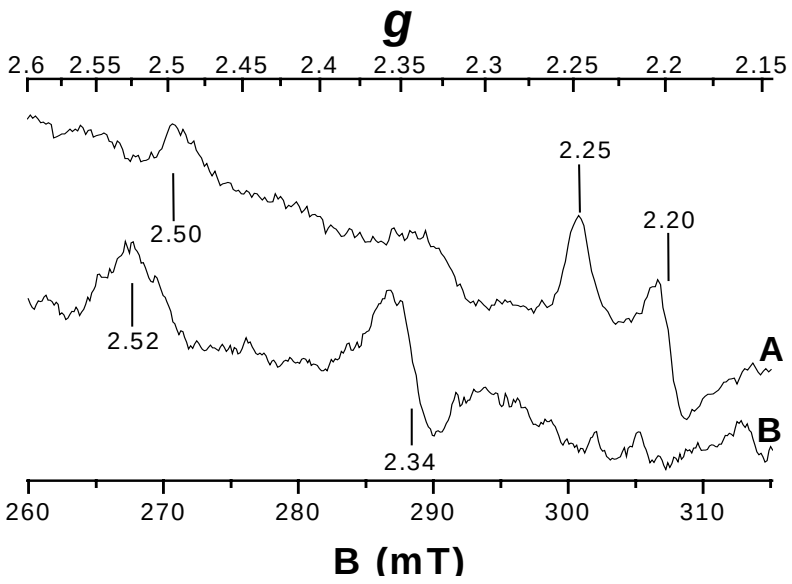

Figure 3-8. Intermediate-field X-band EPR spectra of dithionite-treated mitochondrial preparations *G5* and *G6*. Conditions were as in Figure 3.

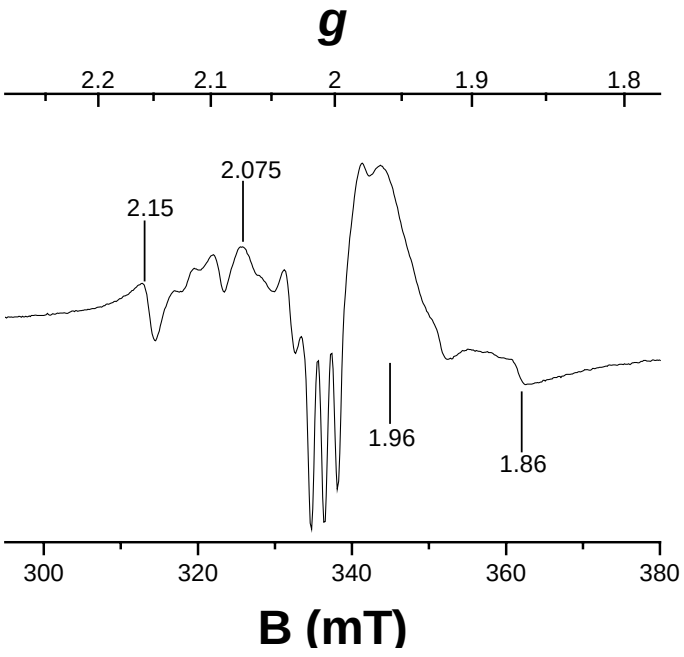

Figure 3-9. High-field X-band EPR spectra of NO-treated mitochondrial preparation *G8*. EPR conditions: microwave frequency, 9.458 GHz, microwave power, 200 μW, modulation amplitude, 10 G, receiver gain, 5.02×10^4, temperature, 10 K.

modest at best. The exception was the presence of the g_{ave} = 2.01 signal which had been observed previously only in spectra from a single EGTA-treated sample (*G3*). The other EPR features of air-oxidized samples (Figure 3-4) were similar to those obtained under completely anaerobic conditions, including the g_{ave} = 1.94 and 1.90 signals. Spin concentrations associated with these signals were also similar. In some but not all air-oxidized samples, the g_{iso} = 2.00 signal was observed. The low–field region of *A4* consisted of a number of low-concentration features but no intense recognizable signals.

Another EGTA-treated sample (*G4*) was exposed to ferricyanide. Again, the g_{ave} = 2.01 signal was present; at the highest spin concentration observed for any sample (6 μM). The g_{ave} = 1.94 and 1.90 signals were present as well. The low-field region displayed a spectrum similar to the as-isolated EGTA-treated samples. An EGTA-treated sample exposed to fumarate exhibited an unusually intense high-spin heme signal with g = 6.4 and 5.3. This signal is similar to that observed in EDTA-treated samples, but with higher intensity.

We also treated our mitochondrial samples with the reductant dithionite, again intending to observe a different group of signals. The low-field region was devoid of signals, as expected from the thermodynamic ability of dithionite to reduce heme groups. The g_{ave} = 1.94 and 1.90 signals were present, with concentrations similar to that observed in as-isolated (and oxidized) samples, even in spectra of the dithionite-reduced sample buffered at pH 8.5. The reduction potential of dithionite declines substantially as pH is lowered, and we anticipated that the intensity of these signals might increase at

pH 8.5 relative to at pH 7.4. A new signal was observed in spectra of the pH 8.5-buffered sample – namely an unresolved absorption-like feature centered at g = 5; this signal almost certainly reflects S = 3/2 $[4Fe\text{-}4S]^{+}$ clusters. At pH 7.4, we see the g_{ave} = 1.94 and 1.90 signals with spin concentrations of 7 and 13 μM, respectively, indicating that the redox state of these species is similar to as-isolated. We do see an additional signal with g = 2.25, 2.20, with a nominal spin concentration. The low-field region was essentially devoid of any signals, suggesting that dithionite reduced the high-spin ferric hemes. At pH 8.5, there is an absorption-like feature between g = 4-6 which is typical of S = 3/2 $[4Fe\text{-}4S]^{+}$ clusters (72). There is a signal with g = 2.52, 2.34, 1.81, which probably arises from a His-Fe-OH heme or cytochrome P450-type center. The low-spin ferric heme species from both the pH 7.4 and 8.5 dithionite samples are shown in Figure 3-8. Also, the spin intensities of the g_{ave} = 1.94 and 1.90 signals have increased to 8 and 17 μM, respectively.

Another preparation was exposed to nitric oxide (NO). This afforded a signal at $g_{\perp}$ = 2.07 and $g_{\parallel}$ = 2.01 (Figure 3-9) which is characteristic of a five-coordinate heme-nitrosyl complex (73). The $g_{\parallel}$ resonance exhibited ^{15}N hyperfine splitting with A = 1.4 mT. The spin concentration associated with this signal (20 μM) was unusually high, and probably reflects the concentration of ferrous heme species present – such species are known to bind to NO to yield signals similar to this signal.

We prepared a sample isolated in EGTA buffers and oxidized in 1 mM ferricyanide (Figure 3-9). The EPR spectrum shows a strong g = 2.01 signal that has a spin concentration of ~6 μM and modest g_{iso} = 2.00 (1 μM), 1.94 and 1.90 signals. The presence of the latter two signals is somewhat surprising because they arise from reduced Fe/S clusters, and ferricyanide should be sufficiently strong to oxidize them. The low-field region shows high-spin heme signals typical of EGTA-treated as-isolated.

The g = 2.01 signal appears under numerous conditions, including O_2 treated, ferricyanide-treated, and fumarate-treated. The g = 2.01 signal is *not* observed in dithionite or all but one of spectra from the as-isolated preps. In general, this signal is observed when samples become oxidized. This is consistent with the oxidative loss of an Fe from an $[4Fe\text{-}4S]^{2+}$ cluster of aconitase. Spin intensities are routinely 5-6 μM, suggesting this concentration for aconitase in intact mitochondria.

CHAPTER IV

MÖSSBAUER SPECTROSCOPY OF INTACT MITOCHONDRIA

Mössbauer spectra were collected on over 20 samples of intact mitochondria. Spectra were collected and analyzed in terms of the physics associated with the technique by Dr. Audria Stubna and Professor Eckard Münck (Department of Chemistry, Carnegie Mellon University). A spectrum from an intact mitochondrial sample isolated in the absence of metal chelators is shown in Figure 4-1A, where three major components can be distinguished. The dominant component is a broad quadrupole doublet with δ = 1.3 mm/sec and ΔE_Q = 3.2 mm/sec, values typical of high-spin ferrous ions. Our estimate of the proportion of spectral intensity represented by this component depends on whether a single Lorenzian line or a Gaussian distribution of such lines is assumed. Since this component most likely reflects a combination of species, a Gaussian distribution is more appropriate, and the simulation assuming this, shown in Figure 4-1A, represents 40% of spectral intensity. In our samples, high-spin ferrous ions could be present in heme prosthetic groups, mononuclear ferrous ions bound to proteins, free Fe^{2+} within the mitochondria, or adventitious Fe^{2+} ions nonspecifically associated with mitochondrial membranes.

The second major component in the spectrum of Figure 4-1A is a quadrupole doublet near the center of the spectrum with δ = 0.45 mm/sec and ΔE_Q = 1.05 mm/sec. Spectral simulation, again assuming a Gaussian distribution of Lorenzian lines, fitted to

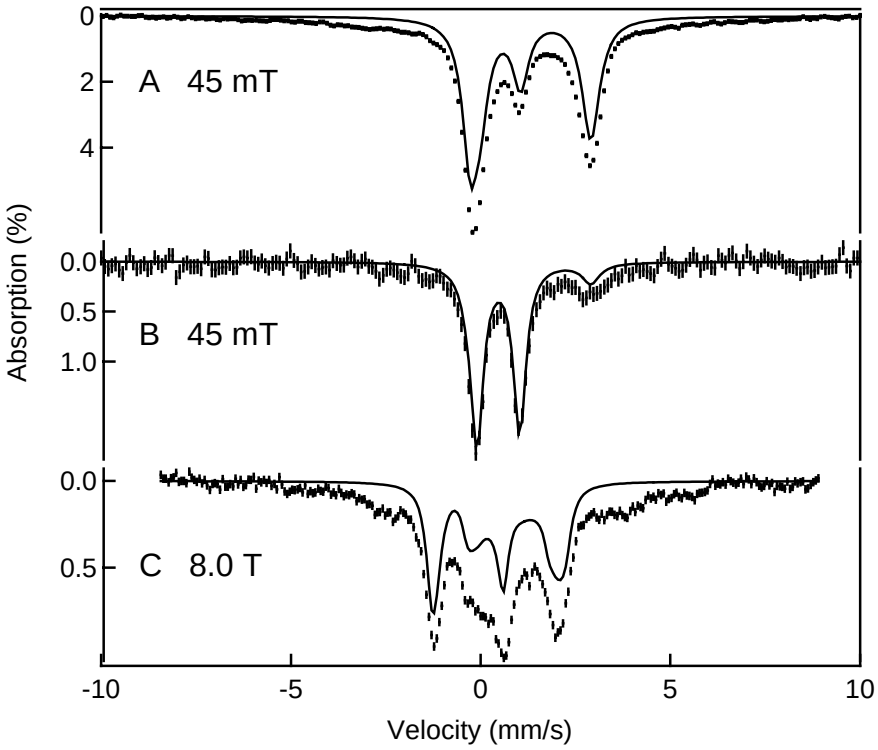

Figure 4-1. Mössbauer spectra of mitochondria. A was prepared in the absence of chelators and collected at 4.2 K in a magnetic field of 45 mT applied parallel to the γ radiation. The mitochondria sample in B and C was exposed to EDTA and collected at 4.2 K and the parallel applied field listed. The solid lines are spectral simulations as described in the text.

~18% of the overall spectral intensity. The remaining broad distribution of magnetic material collapses mainly into a δ = 0.45 mm/s doublet at 150 K, while the Fe^{2+} component experiences non-uniform shifts in ΔE_Q due to their being a population of various excited states (again suggesting that this component arises from numerous different species.) The overall spectral intensity suggests ~3 mM ^{57}Fe in the sample.

An analogous spectrum of mitochondria which had been isolated in the presence of 10 mM EDTA (Figure 4-1B) is substantially different. First, the total spectral intensity indicates less ^{57}Fe in the sample – corresponding to 0.7 M or about 30% of that observed in the unchelated batch. The distribution of Fe also differs substantially, in that the central doublet (with δ = 0.45 mm/sec and ΔE_Q ~ 1.1 mm/sec) now represents 60% of the spectral intensity and the broad high-spin ferrous doublet (with δ = 1.4 mm/sec and ΔE_Q = 3.3 mm/sec) represents 20% of the intensity. The remaining ^{57}Fe absorption arises from iron exhibiting magnetic hyperfine interactions, some or all of which should be EPR active.

The proportion of ^{57}Fe in these three basic forms varied slightly from batch to batch, with the intensity of the central doublet ranging from 50% - 70%, that of the high-spin ferrous component ranging from 10-30%, and that due to magnetic material ranging from 5%-25%. The overall decline in spectral intensity along with the shift in the relative intensities of the different components suggests that the EDTA added during the isolation of mitochondria removed a substantial amount of high-spin ferrous ions from the samples. These ions may have been adventitiously bound and an artifact of our isolation procedure or they may have been chelatable Fe that is required for some

mitochondrial function. This is a difficult issue to resolve, given the large number of mitochondrial functions, some of which are currently poorly understood. In any event, all subsequent ^{57}Fe-enriched mitochondrial samples were isolated in the presence of EDTA or EGTA as this allowed us to observe species that would have otherwise been obscured by the dominant high-spin ferrous component.

Analysis of spectra obtained in a magnetic field of 8 T (Figure 4-1C) indicates that the majority (~ 90%) of the central doublet is diamagnetic (S = 0). This form of Fe has properties expected for $[4Fe\text{-}4S]^{2+}$ clusters as well as for low-spin Fe^{2+} hemes. Unfortunately, these two types of prosthetic groups generally have similar isomer shift and quadrupole splitting parameters, preventing their resolution under these conditions.

The magnetic material observed in spectra from as-isolated mitochondria is probably associated with the species, which exhibit the EPR signals described above. Based on our EPR spectra we can estimate the fraction of Fe present in the form of $[2Fe\text{-}2S]^{+}$ clusters as ~ 10% (30 μM total spin concentration of cluster × 2 Fe/cluster ÷ 600 μM Fe). EPR spin quantification suggests that another ~3% of the iron in our samples are present as high-spin Fe^{3+}. Under certain conditions, another ~3% of the Fe are present as S = 1/2 $[3Fe\text{-}4S]^{+}$ clusters. The sum of these contributions is comparable to the overall percentage of iron in our samples that is magnetic.

At high temperature, oxidized $[2Fe\text{-}2S]^{2+}$ clusters would exhibit a quadrupole doublet distinct from the central doublet (with δ = 0.3 mm/sec and ΔE_Q ~ 0.5 mm/sec), making them observable if > ~10% of the Fe in the sample were in this form. The

absence of such a doublet suggests that < ~10% of the Fe in mitochondria is present as $[2Fe\text{-}2S]^{2+}$ clusters.

We have tried to resolve the contributions of $[4Fe\text{-}4S]^{2+}$ clusters and low-spin, $S = 0$, Fe^{2+} hemes in the as-isolated central doublet by reducing samples with dithionite. Many $[4Fe\text{-}4S]^{2+}$ clusters can be reduced by dithionite, whereas low-spin ferrous hemes would be irreducible. Samples reduced by dithionite at pH 7.4 exhibited Mössbauer spectra that were indistinguishable from those of the as-isolated samples. However, the batch reduced using dithionite at pH 8.5 showed significant reduction. At pH 8.5, the reduction potential for the bisulfite/dithionite couple should be ~130 mV more negative than it is at pH 7.4; we estimate E° ~ -500 mV versus NHE at pH 8.5 for our samples (74). Resulting spectra (Figure 4-2A-B) revealed a more intense magnetic component (the broad feature stretching from -2 to + 2 mm/s) relative to that observed in spectra of as-isolated samples, and a corresponding decline in the central doublet intensity as well as in the high-spin Fe^{2+} doublet (although this feature is no longer easily resolved from the rest of the absorption). Analysis of high-field spectra indicate that the magnetic material is a distribution of many possible species where spectral decomposition of such species is better left to EPR. As discussed in Chapter III, EPR of an analogously-treated sample revealed no substantial increase in the intensity of the $g_{ave} = 1.94$ EPR signal which could have been assigned to $S = 1/2$ $[4Fe\text{-}4S]^{+}$ clusters; however, an absorption-like feature between $g = 4\text{-}6$ which is typical of $S = 3/2$ $[4Fe\text{-}4S]^{+}$ clusters was evident. In any event, the reduction by half of the diamagnetic feature seen at 8 T indicates that this portion of the as-isolated, EDTA-treated sample was due to reducible $S = 0$ [4Fe-

4S]$^{2+}$ clusters. Since this doublet represents ~60% of the as-isolated spectrum, this translates into at least 100 μM of [4Fe-4S]-containing proteins in mitochondria. The other half of the diamagnetic material in the as-isolated sample probably includes low-spin Fe^{2+} heme groups and [4Fe-4S]$^{2+}$ clusters that cannot be reduced by dithionite under the conditions employed.

We have also oxidized samples using both O_2 and ferricyanide, in hopes of oxidizing ferrous ions to their ferric conjugates. Treated in this manner, we expected that low-spin ferrous ions that contributed to the as-isolated central doublet would be converted to low-spin ferric heme groups that would then spectroscopically distinguish themselves from that doublet. We also expected that, under these conditions, some [4Fe-4S]$^{2+}$ clusters would not change oxidation state while others would loose Fe to generate an $S = 1/2$ [3Fe-4S]$^{+}$ cluster. A number of anaerobically-isolated mitochondrial samples were exposed to air for 1 – 2 days and then examined by EPR and Mössbauer. Unexpectedly, such treatment had little effect on the Mössbauer spectra. In contrast, the concentration of the isotropic $g_{iso} = 2.00$ EPR signal, likely due to organic-based radicals, increased upon O_2 exposure. The $g_{ave} = 2.01$ signal, characteristic of $S = 1/2$ [3Fe-4S]$^{+}$ clusters increased in some but not all O_2-treated samples. Given the spin concentrations involved, the contributions of these changes to the Mössbauer spectrum would be minor. Overall, the general lack of spectral changes of both EPR and Mössbauer suggests that mitochondria have a capacity to resist changes in redox state upon exposure to O_2.

We suspected that this buffering-ability was related to the functioning

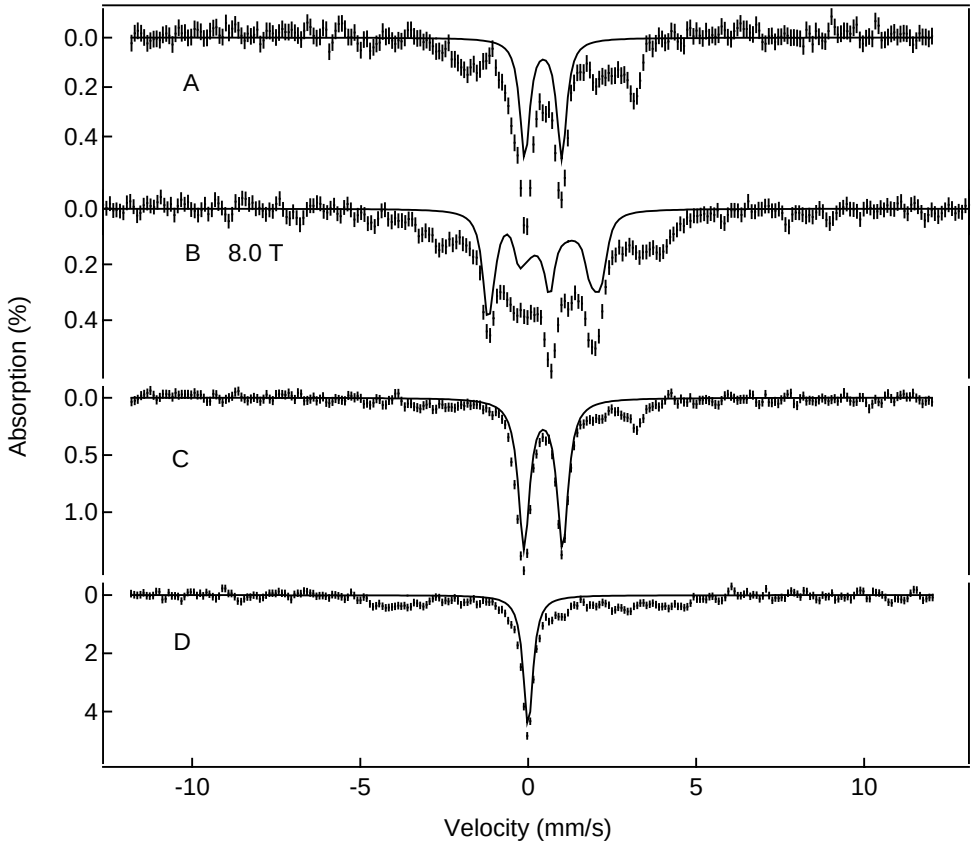

Figure 4-2. Low-temperature (4.2 K) Mössbauer spectra of three different mitochondria samples. A and B are dithionite-treated at pH 8.5, where the solid lines are simulations of a diamagnetic site making up 40% of the total ^{57}Fe absorption. The spectra were taken in a 45 mT magnetic field applied parallel to the γ-beam except in B which is indicated as 8.0 T. Spectrum C is the result of the addition of antimycin A, where the doublet drawn is 65% of the total absorption and D corresponds to the ferricyanide-treated sample as described in the text where 45% of the absorption has been drawn as a $\delta = 0$ mm/s and $\Delta E_Q = 0$ mm/s feature of ferrocyanide.

respiratory electron transport chain, so we blocked this chain using antimycin A, a potent inhibitor of cytochrome bc_1 (75), and then exposed a sample to O_2. With an inactive respiratory complex III, cytochrome *c* could not be reduced, and in turn, cytochrome *c* oxidase could not reduce O_2. The resulting spectrum, shown in Figure 4-2C, was dominated by the central doublet and contained ≤ 10% of the previously discussed high-spin ferrous doublet. These results suggest a more oxidized state overall, but do not explicitly indicate any breakdown of the [4Fe-4S] clusters. Ultimately, a complete understanding of such a sample will involve a detailed study of such a state by EPR spectroscopy.

We have also analyzed EPR and Mössbauer spectra of ferricyanide-oxidized mitochondria. EPR shows an intense feature at g = 2.01, quantifying to a spin concentration of 6 μM; such signals are probably derived from S = 1/2 $[3Fe\text{-}4S]^+$ clusters. Such a signal/cluster is formed when an [4Fe-4S] cluster, such as that of active aconitase, is exposed to ferricyanide. Mössbauer spectra of mitochondria treated with (^{57}Fe-unenriched) ferricyanide (Figure 4-2D) differed dramatically from those of the as-isolated state. specifically, ~45% of the spectral intensity reflected low-spin ferrous ions (actually characteristic of ferrocyanide itself). The remaining ~55% of the intensity reflects broadly distributed magnetic material. The central doublet, which dominated spectra of the as-isolated state, is essentially absent in the spectrum of Figure 4-2D. Thus, treatment with ferricyanide appears to have caused cluster degradation, structural alterations, and perhaps ligand exchange. As such, ferricyanide, a very popular oxidant

for mitochondria, does not appear to act innocently in removing electrons from the clusters present in mitochondria.

CHAPTER V

DISCUSSION

Protein and metal concentrations in mitochondria

The metal content in mitochondria have been reported previously as a *ratio relative* to protein concentration, whereas here we report *apparent absolute* concentrations of protein, Fe, Cu and Mn in packed mitochondria ([protein] ~ 50 mg/ml, [Fe] = 590 μM, [Cu] = 340 μM and [Mn] = 17 μM). These concentrations are *apparent* because our packed mitochondrial samples may not have been pure or devoid of external solution, factors that could distort these values. That being said, we took considerable efforts to obtain tightly-packed high-purity mitochondria. We employed an isolation method known to generate high-purity mitochondria. Resulting gradient-purified solutions were brown, and they consumed O_2 as would be expected for mitochondria capable of respiration. The EM images of this solution are typical of published images of mitochondria (68, 76). After packing, the pelleted material had the consistency of a thick paste, suggesting that most external water had been removed.

Winge and coworkers (77) found 0.65 – 8.1 nmol Cu per mg mitochondrial protein for mitochondria obtained from cells prepared under media supplemented with different levels of Cu. The high-end of this range is comparable to what we observed (6.8 nmol Cu per mg). They also reported Fe/protein ratios ranging from 2.3 - 13 nmol/mg protein, again depending on the media used. Our ratio of 12 nmol Fe/mg protein is again similar to the high-end of this range. They also report Mn levels that

ranged from 0.03 - 0.13 nmol Mn/mg mitochondrial protein. In this case, the ratio we obtained (0.3 nmol Mn per mg protein) is approximately two times higher than their highest value. We attribute this difference to differences in media and growth conditions.

We can also use these relationships to calculate the lower concentration limit for EPR-detectable species in our samples. Using our spectrometer, the detection limit is ~10 nM for sharp isotropic signals and ~100 nM for broad anisotropic ones. This suggests that it would be possible to detect mitochondrially-localized EPR-active species with concentrations as low as 60 – 600 copies per cell ($10^{-8(9)}$ M $\times 10^{-14}$ L $\times$ 6.02×10^{23}). Ghaemmaghami *et al*. reported copy numbers for ~75% of all proteins in yeast (78), and obtained an average value of ~8000 copies/cell. Thus, our technique should be sufficient to detect the majority of EPR-active species contained in yeast mitochondria.

Potential importance of anaerobic isolation

We employed anaerobic isolation methods as a precautionary tactic, in that a number of mitochondrial proteins are inactivated by excess O_2 exposure or under oxidative stress. For example, *in vitro* Fe/S biosynthesis requires anaerobic conditions (79), and it appears that iron is imported into the matrix and delivered to the scaffold proteins in the reduced ferrous state (80). Copper ions are routinely transferred in the reduced cuprous state. Biotin synthase is inactivated by O_2 (81). Maximal ferrochelatase activity is observed under anaerobic conditions (82). The labile iron in the [4Fe-4S] cluster of aconitase dissociates (thereby inactivating the enzyme) under oxidizing conditions (83). With the exception of ferrochelatase, these O_2-sensitive enzymes are

located in the matrix; however, ferrochelatase receives ferrous ions from the matrix. Lill, and independently Henze and Martin, suggest that the matrix is the most anaerobic compartment in O_2-respiring cells (84). Given the predominant role of O_2 in reactions occurring within mitochondria, this might seem counterintuitive. However, the O_2-consuming reactions occur at the IM, which encapsulates the matrix (85). We suspect that these reactions occur fast enough to effectively remove from the matrix any O_2 that diffuses into this region.

Adventitious Fe and Mn

The hyperfine-split signal observed in the $g = 2$ region of our as-isolated samples is typical of adventitious or weakly bound Mn^{2+} ions and we assign it as such. For the EDTA and EGTA treated samples, this signal vanishes, but the metal analysis indicates a small concentration of Mn (>10 μM) is retained by the mitochondria. This amount of adventitiously bound Mn(II) may be near the detection limit for our EPR instrument. There are a few Mn-containing proteins found in yeast mitochondria that could account for the amount of Mn detected in our metal analyses. The matrix protein Sod2p is one such protein that is found in mitochondria (78, 86, 87). Based on $S = 5/2$ simulations using the known parameters for Sod2p [$D = 0.348$ cm^{-1}, $E/D = 0.026$ (88)], our calculations indicate that we could detect a minimum concentration of 10 μM Mn(II) ions from Sod2p, which is within the error of the concentration of Mn detected in our metal analyses. Another possibility is the IM Mn-chaperone Mtm1p, but we suspect that this protein is present in very low concentrations.

The $g = 4.3$ signal probably arises from Fe^{3+} ions that are adventitiously bound to mitochondrial proteins or phospholipids. Our studies indicate that this type of iron is chelatable, suggesting that it resides in a region that can be accessed by EDTA and EGTA such as the outer face of the OM. The presence of aqueous Fe^{3+} ions suggests that this region has a rather high potential. Previous reports have used the $g = 4.3$ signal as a quantitative diagnostic for cellular damage (89), but our study suggests that caution should be applied in these interpretations, in that this signal may also arise from Fe^{3+} peripherally associated with these organelles.

Species containing Fe/S clusters

The dominant spectral feature with EDTA- and EGTA-treated samples was the $g_{ave} = 1.94$ signal. The signal also appears present in spectra of the as-isolated samples, though it is dominated by the Mn^{2+} signal. We assign it to the $[2Fe\text{-}2S]^{+}$ cluster of succinate dehydrogenase. This cluster exhibits an EPR signal with *g*-values nearly identical to those observed here (90). Others have observed a similar signal in their mitochondrial preparations, and have assigned it similarly (91). Nevertheless, we regard this assignment as tentative because $g_{ave} = 1.94$ signals are characteristic of many $[4Fe\text{-}4S]^{+}$ and $[2Fe\text{-}2S]^{+}$ containing proteins and we cannot exclude the possibility that the observed $g_{ave} = 1.94$ signal arises from a mitochondrial protein other than Sdh2p (or from a mixture of signals with similar *g*-values).

The saturation properties of the $g_{ave} = 1.94$ signal ($P_{1/2} = 57$ mW at 10 K) are similar to those reported for the succinate dehydrogenase $[2Fe\text{-}2S]^{+}$ cluster but only

under conditions *where the [4Fe-4S] cluster in the same enzyme is reduced to the 1+ state* (92). When the [4Fe-4S] cluster is oxidized to the diamagnetic 2+ state, the saturation behavior of the $[2Fe\text{-}2S]^{+}$ cluster differs substantially ($P_{1/2}$ = 0.63 mW). The observed saturation behavior indicates that the [4Fe-4S] cluster is reduced to the 1+ core oxidation state in our samples. Since $E^{\circ\prime}$ for this cluster is -270 mV (93, 94), this implies that the potential of solution for which this cluster is in redox-equilibrium is at or below this value.

The g_{ave} = 1.90 signal is similar to that exhibited by the isolated Rieske $[2Fe\text{-}2S]^{+}$ protein (92), and we assign it as such. $E^{\circ\prime}$ for the 2+/1+ redox couple is + 280 mV (95). The protein is part of the cytochrome bc_1 complex, which is located in the IM, but the Rieske protein itself is tethered to the rest of the complex and extends into the IMS. This cluster transfers electrons to the IMS protein cytochrome *c*, suggesting that it will be in redox equilibrium with the IMS. Assuming this, the presence of this signal suggests that the potential of the IMS is less than +280 mV in our samples.

The g_{ave} = 2.02 signal observed in sample *G3*, some O_2-oxidized samples, and in ferricyanide-treated samples is similar in *g*-values and lineshape to that exhibited by the inactive $[3Fe\text{-}4S]^{+}$ form of the aconitase cluster (96, 97) and we assign it to this enzyme. The absence of this signal in our as-isolated samples suggests that the anaerobic conditions maintained this cluster in the active $[4Fe\text{-}4S]^{2+}$ state. Of the as-isolated samples, only *G3* may have been prepared under slightly more oxidizing conditions.

Species containing hemes

As-isolated samples reproducibly contained two $S = 5/2$ species, with $E/D = 0.042$ (g = 6.8, 5.0) and $E/D \sim 0$ ($g = 6$). EDTA-treated samples reproducibly contain another $S = 5/2$ species with $E/D = 0.024$ ($g = 6.4, 5.3$) while EGTA-treated samples reproducibly contained the species with $E/D \sim 0$ and $E/D = 0.024$ but not the one with $E/D = 0.042$. Spectra containing what appears to be these latter two signals associated with EGTA-treated samples have been reported for an intermediate redox state of the heme a_3:Cu_B active site of cytochrome *c* oxidase (98). In this state, the Cu_B is probably in the diamagnetic Cu^+ state while heme a_3 is high-spin Fe^{3+} and is responsible for the signal observed. Interestingly, the reported spectra show not only the same *g*-values as those observed for our samples, but also roughly the same *ratio* of the two signals. In previous studies, the combined quantified intensity of these signals corresponded to 35% - 40% of the cytochrome oxidase concentration, suggesting that this respiratory complex is present at a concentration of ~6 μM. Starting from the oxidized state, this signal appeared and disappeared in accordance with midpoint potentials of +380 mV and +230 mV, respectively (99). The presence of this signal in our samples suggests that the a_3:Cu_B site is in redox equilibrium with a region having a potential between these values.

The remaining high-spin heme signal may be due to the high-spin ferric heme *b* in the IMS cytochrome *c* peroxidase, as similar *g*-values have been reported (100-102). The particular degree of rhombic distortion can depend on pH or subtle structural changes. The redox potential for the Fe^{3+}/Fe^{2+} couple of this protein is -182 mV at pH 7

(103) suggesting that in our samples, the potential of the IMS region is greater than this value.

Organic radical species

The isotropic g_{iso} = 2.00 signal has *g*-values and saturation properties typical of organic radicals, and we assign this signal to the population of such radicals in our samples. Possible sources include the semiquinone states of flavins and ubiquinone, and perhaps reactive oxygen species. Given the preponderance of ubiquinone (0.6-4.0 μmols/g mitochondrial protein) (104) and flavin-containing proteins (see *Introduction*), we were rather surprised that the spin concentrations of the g_{iso} = 2.00 signal were so low. This suggests that there are only 200-1200 stable radical moieties present in the mitochondrial volume per cell under our growth and isolation conditions. Recall that our cells were grown under *respiratory* conditions but mitochondria were isolated *anaerobically*. Radical species generated during cell growth may have decayed during the period when our mitochondria were isolated.

New mitochondrial EPR signal

Our samples exhibited an EPR signal with g_{ave} = 2.04 that arises from an unknown species contained in these organelles. We have considered that the g_{ave} = 2.04 signal originates from thiyl radicals, as these species exhibit similar broad $g_{||}$ features in this region (105). Such species might play a role in biotin synthesis (105). However, we regard this as unlikely because: (1) the $g_{\perp}$ feature for known thiyl radicals is always

observed to be much stronger relative to the $g_{||}$ than what is observed for this signal; (2) the $P_{1/2}$ of the g = 2.08 feature (1 mW) is a factor of 10 lower than the $g_{||}$ feature of thiyl radicals, and our signal does not appear to display the saturation anisotropy typical of thiyl radicals; and (3) the g_{ave} = 2.04 signal is stable at room temperature. Possibly this signal originates from a spin interaction with an Fe/S cluster; such spin interactions have been previously observed from respiratory complex II. However, this signal is not similar to the g = 2.06 signal from respiratory complex II assigned to an Fe/S cluster interaction (106), since we do not observe the associated g = 1.84 resonance. Nor does it compare favorably with the g = 2.04 signal observed from respiratory complex II and assigned to an Fe/S-radical interaction (97).

Implications from the absence of signals

We were surprised by the lack of EPR signals due to low-spin ferric hemes; such signals are typically found at g_z = {2.6-2.4}, g_y = {2.5-2.2}, and g_x = {1.91-1.85} (107). A few minor species (at g = 2.25 and 2.20 and at g = 2.5 and 2.34) were observed in dithionite-reduced samples, but the origin of these signals is unclear. Given the presence of many low-spin ferric heme groups in mitochondria (cytochrome *c*, cytochrome c_1, heme *a* in cytochrome *c* oxidase, all of which should be in redox equilibrium with the IMS), it seems unlikely that their combined concentration would not have been sufficient to be observed. Previous studies report concentrations of 0.15-0.3 μmol/g protein for cytochromes *a*, 0.2-0.4 μmol/g protein for cytochrome *c*, 0.07-0.25 μmol/g protein for cytochrome c_1 (107), which corresponds to easily detectable concentrations in our

samples with ~50 mg/ml protein concentration. Since $E^{\circ\prime}$ = +230 mV for cytochrome c_1 (108), +290 mV for cytochrome *c* (108), and +255 mV for heme *a* (109), one possibility is that the potential of the IMS space in our samples was below ca. +230 mV, rendering these centers ferrous and EPR-silent.

We also did not observed signals characteristic of Cu^{2+} ions, even though, by chemical analysis, our samples contained copper at sufficiently high concentrations. The lack of such signals suggests that the vast majority of copper in our samples are in the diamagnetic Cu^{+} state. The most well-known Cu centers in mitochondria are the Cu_A and Cu_B sites in cytochrome *c* oxidase. Oxidized Cu_A exhibits an EPR signal with g = 2.17 (110), but no such signal was observed. $E^{\circ\prime}$ for Cu_A is +240 mV (111). This center should be in redox equilibrium with the IMS, as it functions to accept electrons from cytochrome *c*. Since there appears to be sufficient cytochrome *c* oxidase in our samples to be observed, this implies that the potential of the IMS is less than ca. +230 mV. Mitochondria also contain a number of copper chaperones, but such centers appear stable only in the diamagnetic Cu^{+} state (112, 113). Winge has suggested that ~ 90% of the Cu in yeast mitochondria is not associated with proteins and is located in the matrix in a Cu^{+} form. Our results are consistent with this, both in terms of the concentration of copper observed and the absence of Cu^{2+}-based EPR signals.

Implications of spin quantifications

The measured spin concentrations could be interpreted further if it were assumed that: a) they represent the concentrations of the associated protein in the sample; b) all

such protein molecules are associated with the complex for which they have been reported to be associated; and c) the stoichiometry of complex association is as reported. Under these assumptions, a 4 μM spin concentration for the g_{ave} = 1.94 signal from the $[2Fe\text{-}2S]^{+}$ cluster of Sdh2p would indicate that respiratory complex II would be present at this concentration. Since this complex also contains one [4Fe-4S] cluster, one [3Fe-4S] cluster, and one heme, 40 μM of Fe would be thus accounted for. Similarly, an 8 μM spin concentration for the g_{ave} = 1.90 signal from the $[2Fe\text{-}2S]^{+}$ cluster of Rip1p would indicate this concentration for respiratory complex III. Since this complex also contains three hemes (b_L, b_H, and c_1), this accounts for another 40 μM Fe. The spin concentration of the signals from cytochrome *c* peroxidase suggests that this protein is present at a concentration of ~5 μM. In this example, the concentration of these three species would account for ~ 14% of the Fe in yeast mitochondria (85 μM/590 μM × 100).

Electrochemical potentials of mitochondrial compartments

It would be impossible to interpret our results if forced to assume that all redox centers in our mitochondrial samples sensed the same electrochemical potential. The fact that the $[2Fe\text{-}2S]^{+}$ cluster of succinate dehydrogenase was observed with the indicated saturation properties suggests that the potential of the solution with which this cluster is in redox equilibrium was less than approximately -270 mV. In contrast, we see the oxidized Fe^{3+} heme from cytochrome *c* peroxidase, which implies a solution potential greater than -190 mV (and the presence of adventitious Fe^{3+} implies even more positive potentials). The solution potential of a single compartment cannot simultaneously be > -

190 mV and < -270 mV. This requires that we assume different solution potentials for different compartments. The matrix (in redox equilibrium with the succinate dehydrogenase signals) may have a potential less than -270 mV while the IMS may have a potential between +230 and -190 mV. When oxygenated mitochondria are "energized" by adding NADH, the IMS and matrix are known to have a "membrane potential" of ~200 mV, with the matrix negative (114). The presence of a membrane potential in the absence of NADH and O_2 would suggest that mitochondria are energized even when not engaged in respiration; i.e. the energized state is a basal or stationary state of mitochondria rather than a steady-state situation achieved only when electrons pass through respiratory complexes. In previous studies, mitochondria have been "energized" by adding NADH to aerobic mitochondria (115), leaving it ambiguous as to whether forming a membrane potential required only reducing conditions or steady-state turnover conditions.

Implications from Mössbauer results

The combined use of EPR and Mössbauer spectroscopy along with analytical characterization allows us to estimate the distribution of Fe in yeast mitochondria. *No such distribution has been reported previously*. We must stress that these estimates are preliminary and that our numbers are "soft". Overall, however, we have a fairly consistent picture of what types of Fe environments are found in these organelles. First, we see a significant influence upon treating of our samples with chelators during the isolation procedure, suggesting that if no such chelators are used during isolation, a

substantial fraction of the observed Fe actually reflects chelatable Fe (perhaps adventitiously bound to the mitochondrial outer membrane). For samples treated with chelators, the overall Fe concentration in mitochondria is ~ 600 μM.

Approximately 60% of this Fe gives rise to a diamagnetic "central doublet" which has parameters typical of $[4Fe\text{-}4S]^{2+}$ clusters and low-spin ferrous hemes. Treatment with dithionite at pH 8.5 causes approximately half of this material to become reduced to the $[4Fe\text{-}4S]^{+}$ state (with predominately $S = 1/2$ but also some $S = 3/2$ form). Thus, at a minimum, our mitochondria contain ~ 100 μM of [4Fe-4S]-containing proteins (corresponding to ~ 400 μM Fe). Approximately 20 μM of this is due to aconitase (and/or homoaconitase).

Approximately 25% (~150 μM) of the Fe in chelated mitochondria is in the form of high-spin ferrous ions. Our EPR analysis suggests that at least ~30 μM of this is present as high-spin heme groups, leaving no more than ~140 μM due to other high-spin ferrous ions. These later ions might be found in ferrochelatase (Hem15p), frataxin (Yfh1p), other Fe carriers/transporters and other forms not currently identified.

Mössbauer spectra of as-isolated mitochondria indicate that ~15% of the Fe is magnetic and in half-integer spin states. By EPR, this would appear to include the high-spin heme signals from cytochrome oxidase and cytochrome *c* peroxidase (~4 μM), the low-spin ferric hemes (totaling ~ 2 μM), the $[2Fe\text{-}2S]^{+}$ cluster of the Rieske protein of cytochrome bc_1 (20 μM) and the $[2Fe\text{-}2S]^{+}$ cluster from succinate dehydrogenase (10 μM). The $[4Fe\text{-}4S]^{+}$ cluster of the latter enzyme might also contribute to the spectra.

Summing these EPR contributions affords ~100 μM Fe, or ~15% of the total Fe, matching the half-integer magnetic contribution observed by Mössbauer spectroscopy.

Thus far, the Mössbauer spectra shows little evidence of $[2Fe\text{-}2S]^{2+}$ clusters; we estimate that less than 10% of the Fe is in this form, corresponding to less than 35 μM of $[2Fe\text{-}2S]^{2+}$-containing proteins in our as-isolated samples. This is actually quite consistent with our inventory of Fe-containing proteins in mitochondria; such clusters should be found only in Yah1p (2 μM), the scaffold Fe/S proteins (4 μM combined), lipoic acid synthase (0.3 μM) and biotin synthase (0.1 μM). Collectively, 7 μM protein translates into 2% of the total Fe, consistent with our inability to observe such features in mitochondrial Mössbauer spectra.

Similar to the situation with the EPR samples, a large quantity of adventitious Fe is observed in Mössbauer spectra when metal chelators are not included in all isolation buffers. A comparison of the spectra in Figure 4-1 (no chelator) with the spectra in Figure 4-2 reveals a shift not only in the Fe concentration of the samples but also the proportion of the centers. There are many published reports in which the Fe content of isolated mitochondria has been measured, and important conclusions are often based on these measurements. Our results raise the possibility that a significant portion of that Fe is actually adventitiously bound Fe^{2+}, and it emphasizes a clear advantage of our approach, i.e. we can distinguish different types of Fe in a mitochondrial sample.

CHAPTER VI

SUMMARY AND FUTURE STUDIES

The major contributions of this study are:

- *New method to observe EPR and Mössbauer of intact mitochondria*: A new tight-packing method for preparing intact mitochondria from yeast is described which allows high-quality (quantifiable) EPR and Mössbauer spectra of these organelles to be obtained for the first time.
- *Estimate of absolute protein and metal concentrations in mitochondria:* Preliminary estimates for the absolute protein and metal (Fe, Cu, and Mn) concentrations contained within these organelles synthesized by respiring cells are reported for the first time.
- *Effect of EDTA and EGTA:* The effect of adding these metal chelators during the isolation of mitochondria is reported. Their inclusion was associated with the loss of signals associated with Fe and Mn but there was no significant effect on O_2 consumption.
- *EPR signals and spin concentrations:* Recognizable signals were observed from succinate dehydrogenase, the Rieske Fe/S protein, cytochrome *c* oxidase, aconitase, and cytochrome *c* peroxidase. Each of these proteins appears to be present at concentrations between 1 – 20 μM. A signal with low-spin concentration (0.2 μM) from organic radicals was observed.

- *New signal discovered:* A signal with g_{ave} = 2.04 was identified, suggesting the presence of previously unidentified EPR-active species in yeast mitochondria.
- *Expected signals not observed:* No definitive low-spin ferric heme signals or signals from Cu^{2+} ions were observed, probably because the redox state of the mitochondria was too low.
- *Electrochemical compartmentalization in mitochondria:* Consideration of the redox potentials of species which exhibit EPR signals and those that did not suggested that the potential of different regions of the mitochondria are different, with the matrix being substantially more negative in potential than the intermembrane space.
- *Resolution of Mössbauer-active centers in intact mitochondria*. The distribution of Fe-centers in yeast mitochondria was described in terms of *groups* of such centers. These organelles predominately contain $[4Fe\text{-}4S]^{2+}$ clusters, most of which are located in the matrix. The second-most abundant type of Fe-center is high-spin ferrous ions. EPR studies identified some $[2Fe\text{-}2S]^{+}$ clusters and high-spin ferric hemes. The presence of low-spin ferrous and ferric hemes cannot be ruled out, but their presence was obscured. There was no evidence for $[2Fe\text{-}2S]^{2+}$ clusters. When isolated in the absence of metal chelators, mitochondria contain a substantial quantity of adventitious Fe (III) and Mn (II).

The body of work described herein represents the most comprehensive investigation of intact mitochondria from *Saccharomyces cerevisiae* using EPR and

Mössbauer spectroscopies supplemented with quantitative protein and transition metal analysis to date. The use of intact mitochondria versus organellar extracts or individual proteins, combined with the anaerobicity of the isolation procedure, allowed for a unique, systems biology inspired approach for studies that more faithfully resemble the conditions experienced by the organelle *in vivo*. Mitochondrial fractions were grown under respirative conditions and isolated in the presence or absence of divalent metal chelators. EDTA, a membrane permeable chelator, is capable of entering mitochondria while EGTA, which is membrane impermeable, could only chelate metal ions located on the periphery of the organelles. EPR and Mössbauer samples isolated in the presence of chelators versus those isolated in their absence appear significantly different.

The EPR spectra of as-isolated mitochondria, i.e. those isolated in the absence of EDTA and EGTA, contain a significant six-line hyperfine pattern in the high field, "g = 2" region of the spectrum. Its g-values, linewidths, and line spacings are consistent with the presence of a high-spin Mn^{2+} species. This feature dominates the high field portion of the as-isolated EPR spectra. The low field portion of the as-isolated spectra are dominated by a high-spin, mononuclear Fe^{3+} center assigned as adventitious Fe not coordinated in any protein active sites. The use of EDTA and EGTA eliminate the Mn^{2+} feature and reveal the presence of species such as Fe/S clusters, organic-based radicals, and other species. Specifically, species consistent with the presence of the $[2Fe\text{-}2S]^{+}$ clusters of succinate dehydrogenase (g = 2.026, 1.934, 1.913) and the Rieske protein from cytochrome bc_1 (g = 2.025, 1.897, 1.784) were identified and have been tentatively assigned. Additionally, a carbon- or oxygen-based radical centered at g = 2.00 was

identified and tentatively assigned. The low field portion of these spectra contain three species with spectral parameters consistent with high-spin Fe^{3+} heme centers, including the intermembrane space protein cytochrome *c* peroxidase (g = 6.8, 5.0) All of these signals were quantified using QPOWA or software developed by a collaborator (Michael P. Hendrich). The absolute concentrations of the potentially EPR-active transition metals in the samples, namely Fe, Cu, and Mn, were quantified using AAS.

A comparison of the as-isolated EPR mitochondrial samples versus those isolated in the presence of chelators suggests the use of chelators is valuable in that more species can be discerned from the spectra. The major EPR-active species removed from the use of chelators, the Mn^{2+} center, does not appear to be affiliated with any mitochondrial proteins such as Mn-SOD and is tentatively assigned as adventitious Mn^{2+}. Moreover, the chelators do not inhibit the ability of the mitochondria to remove O_2 from their surroundings, as demonstrated by oxygen consumption assays.

A variety of reductants and oxidants were incorporated in an attempt to reveal EPR signals from species that are not spectroscopically active under our anaerobic isolation procedure. Surprisingly, the spectra of many redox-treated EPR samples differed little from the samples prepared in the absence of reductants or oxidants. The spectra of samples exposed to air at 4°C, whether isolated in the absence or presence of the aforementioned chelators, appear very similar to their anaerobically-prepared counterparts. This result suggests the organelles have some homeostatic mechanism to protect themselves against changes in the redox environment in which they reside. However, some of the redox titrations resulted in EPR signals not observed in untreated

samples. Mitochondria incubated in 10 mM dithionite exhibited features consistent with the presence of two low-spin ferric heme proteins. One species (g = 2.52, 2.34, 1.81) is most consistent with a OH-Fe-His heme site or cytochrome P450-type center. The cytochrome proteins found in the oxidative phosphorylation complexes of the inner membrane are the most likely contributors of these signals. These signals each had a minor spin concentration. Treatment of mitochondria with 1 mM ferricyanide resulting in a signal (g = 2.02, 2.01, 2.00) that is tentatively assigned to the inactive, [3Fe-4S] form of Aco1p and Aco2p, the homologous yeast aconitases localized in the mitochondrial matrix. This signal had a spin concentration of 6 μM. Additionally, the ferricyanide-treated sample exhibited a more significant isotropic, g = 2 radical species compared to untreated samples (~1 μM compared to less than 200 nM for as-isolated samples).

The use of Mössbauer spectroscopy in tandem with EPR can synergistically provide greater insight into Fe-containing species (116). As with the EPR samples described previously, samples for Mössbauer spectroscopy were prepared either in the presence or absence of chelators, with both EDTA and EGTA utilized. The sample prepared in the absence of chelators had an ^{57}Fe concentration of 3.0 mM. A significant portion of the Fe is in the form of high-spin Fe^{2+} (FC), and likely results from ferrous ions not coordinated to any protein centers. The use of EDTA and EGTA greatly reduced the concentration of ^{57}Fe in the samples, with a range of 0.7 to 1.4 mM. The FC in the samples was the species most affected in the samples prepared with chelators, suggesting this feature is largely adventitious Fe. However, the use of EDTA and EGTA

greatly enhanced the central doublet (CD), which likely contains $[4Fe\text{-}4S]^{2+}$ clusters and low-spin ferrous hemes. Although these two species are not currently resolvable, ongoing studies should allow for the discernment of the two in the future.

Redox treatment of intact mitochondria was performed in an effort to extract additional information of the Fe centers in the samples described in this work. Samples prepared from air-oxidized mitochondria have similar features to matched samples prepared under strictly anaerobic conditions, although the concentration of ^{57}Fe in the samples decreases, in certain samples by 50%. One explanation for this phenomenon may be that the mitochondria are effusing nonessential Fe, although other possibilities such as proteolysis or degradation of certain Fe-containing centers are also possibilities. The use of dithionite showed little effect for the sample incubated at pH 7.4 compared to untreated samples. However, the sample incubated in dithionite, pH 8.5 appeared more reduced compared to untreated samples. The use of the cytochrome bc_1 inhibitor antimycin A resulted in a spectrum dominated by CD and devoid of much of the MM and FC found in untreated samples. Ferricyanide treatment of intact mitochondria resulted in a spectrum comprised of two components, low-spin Fe^{3+} as the dominant species and MM also present.

In addition to the results and ongoing studies described above, further incorporation of genetics will be called upon to provide insight into the effects of deletion or overexpression of proteins relevant to mitochondrial iron homeostasis, particularly those involved in Fe/S cluster biosynthesis and export. A sample from a mutant yeast strain deficient in the adrenodoxin Yah1p has also been characterized. The

function of this protein, essential for Fe/S cluster formation, is as an electron transport protein for the reduction of nascent Fe/S clusters. As expected, the sample is devoid of features consistent with Fe/S clusters and instead contains a significant amount of high-spin Fe^{2+} ions. This feature is similar to the FC found in mitochondrial samples isolated in the absence of chelators. Such a result is expected in mitochondria capable of importing Fe but unable to incorporate it into the synthesis of nascent Fe/S clusters.

Samples from a strain deficient in the yeast frataxin protein, Yfh1p, are currently being prepared. Additional studies will focus on mitochondrial EPR and Mössbauer samples prepared from an overexpression strain of Yfh1p. These studies should provide further insight into the role of frataxin in iron homeostasis, particularly as it relates to the spectroscopically active species characterized in this work. EPR and Mössbauer spectroscopies will also be used to investigate mitochondrial samples prepared from cells grown under fermentative conditions. These studies will provide a clearer understanding of the effects of carbon source and growth conditions on the mitochondrial "EPR-ome" and the iron-containing centers through Mössbauer spectroscopic studies.

REFERENCES

1. Lill, R., Fekete, Z., and Rotte, C. (2005) Why are mitochondria essential for life? *IUBMB Life 57*, 701-703.
2. Egner, A., Jakobs, S., and Hell, S. W. (2002) Fast 100-nm resolution three-dimensional microscope reveals structural plasticity of mitochondria in live yeast, *Proc. Natl. Acad. Sci. USA 99*, 3370-3375.
3. Atamna, H., Walter, P. B., and Ames, B. N. (2002) The role of heme and iron-sulfur clusters in mitochondrial biogenesis, maintenance, and decay with age, *Arch. Biochem. Biophys. 397*, 345-353.
4. Rolo, A. P., and Palmeira, C. M. (2006) Diabetes and mitochondrial function: Role of hyperglycemia and oxidative stress, *Toxicology and Applied Pharmacology 212*, 167-178.
5. Rosenberg, P. (2004) Mitochondrial dysfunction and heart disease, *Mitochondrion 4*, 621-628.
6. Webb, C. T., Gorman, M. A., Lazarou, M., Ryan, M. T., and Gulbis, J. M. (2006) Crystal structure of the mitochondrial chaperone TIM9 center dot 10 reveals a six-bladed alpha propeller, *Molecular Cell 21*, 123-133.
7. Han, J., Thompson-Lowrey, A. J., Reiss, A., Mayorov, V., Jlia, H., Biousse, V., Newman, N. J., and Brown, M. D. (2006) OPA1 mutations and mitochondrial DNA haplotypes in autosomal dominant optic atrophy, *Genetics in Medicine 8*, 217-225.

8. Walter, P.B., Knutson, M. D., Paler-Martinez, A., Lee, S., Xu, Y., Viteri, F. E., and Ames, B. N. (2002) Iron deficiency and iron excess damage mitochondria and mitochondrial DNA in rats, *Proc. Natl. Acad. Sci. USA 99*, 2264-2269.

9. Gonzalez-Cabo, P., Vazquez-Manrique, R. P., Garcia-Gimeno, M. A., Sanz, P., and Palau, F. (2005) Frataxin interacts functionally with mitochondrial electron transport chain proteins, *Hum. Mol. Gen. 14*, 2091-2098.

10. Bonagura, C. A., Bhaskar, B., Shimizu, H., Li, H. Y., Sundaramoorthy, M., McRee, D. E., Goodin, D. B., and Poulos, T. L. (2003) High-resolution crystal structures and spectroscopy of native and compound I cytochrome *c* peroxidase, *Biochemistry 42*, 5600-5608.

11. M. R. Moore and A. Goldberg, "Normal and abnormal [heme] biosynthesis" in *Iron in Biochemistry and Medicine*, A. Jacobs and M. Worwood, eds., Academic Press, London, 1974.

12. Lesuisse, E., Santos, R., Matzanke, B. F., Knight, S. A. B., Camadro, J. M., and Dancis, A. (2003) Iron use for heme synthesis is under control of the yeast frataxin homologue (Yfh1), *Human Molecular Genetics 12*, 879-889.

13. Ferreira, G. C., Franco, R., Lloyd, S. G., Moura, I., Moura, J. J. G., and Huynh, B. H. (1995) Structure and function of ferrochelatase, *J. Bioenerg. Biomem. 27*, 221-229.

14. Gerber, J., Lill, R. (2002) Biogenesis of iron-sulfur proteins in eukaryotes: Components, mechanism, and pathology, *Mitochondrion 2*, 71-86.

15. Beinert, H., Holm R. H., and Münck. E. (1997) Iron-sulfur clusters: Nature's modular, multipurpose structures, *Science 277*, 653-659.

16. Mühlenhoff, U., Richhardt, N., Gerber, J., and Lill, R. (2002) Characterization of iron-sulfur protein assembly in isolated mitochondria, *J. Biol. Chem. 277*, 29810-29816.

17. Foury, F., and Roganti, T. (2002) Deletion of the mitochondrial carrier genes *MRS3* and *MRS4* suppresses mitochondrial iron accumulation in a yeast frataxin-deficient strain, *J. Biol. Chem.* 277, 24475-24483.

18. Li, L. T., and Kaplan, J. (1997) Characterization of two homologous yeast genes that encode mitochondrial iron transporters, *J. Biol. Chem.* 272, 28485-28493.

19. Schilke, B., Voisine, C., Beinert, H., and Craig, E. (1999) Evidence for a conserved system for iron metabolism in the mitochondria of *Saccharomyces cerevisiae*, *Proc. Natl. Acad. Sci. USA 96*, 10206-10211.

20. Tong, W. H., Jameson, G. N. L., Huynh, B. H., and Rouault, T. A. (2003) Subcellular compartmentalization of human Nfu, an iron-sulfur cluster scaffold protein, and its ability to assemble a [4Fe-4S] cluster, *Proc. Natl. Acad. Sci. USA 100*, 9762-9767.

21. Mühlenhoff, U., Gerber, J., Richhardt, N., and Lill, R. (2003) Components involved in assembly and dislocation of iron-sulfur clusters on the scaffold protein Isu1p, *EMBO J. 22*, 4815-4825.

22. Pelzer, W., Mühlenhoff, U., Diekert, K., Siegmund, K., Kispal, G., and Lill, R. (2000) Mitochondrial Isa2p plays a crucial role in the maturation of cellular iron-sulfur proteins, *FEBS Letters 476*, 134-139.

23. Barros, M. H., and Nobrega, F. G. (1999) *YAH1* of *Saccharomyces cerevisiae*: A new essential gene that codes for a protein homologous to human adrenodoxin, *Gene 233*, 197-203.

24. Xia B., Cheng H., Bandarian V., Reed G. H., and Markley J. L. (1996) Human ferredoxin: Overproduction in *Escherichia coli*, reconstitution *in vitro*, and spectroscopic studies of iron-sulfur cluster ligand cysteine-to-serine mutants, *Biochemistry 35*, 9488-9495.

25. Kispal, G., Steiner, H., Court, D. A., Rolinski, B., and Lill, R. (1996) Mitochondrial and cytosolic branched-chain amino acid transaminases from yeast, homologs of the *myc* oncogene-regulated Eca39 protein, *J. Biol. Chem. 271*, 24458-24464.

26. Lange, H., Lisowsky, T., Gerber, J., Mühlenhoff, U., Kispal, G., and Lill, R. (2001) An essential function of the mitochondrial sulfhydryl oxidase Erv1p/ALR in the maturation of cytosolic Fe/S proteins, *EMBO Reports 2*, 715-720.

27. Hutcheon, G. W. and Bolhuis, A. (2003) The archaeal twin-arginine translocation pathway, *Biochemical Society Transactions 31*, 686-689.

28. Barros, M. H., Johnson, A., and Tzagoloff, A. (2004) *COX23*, a homologue of *COX17*, is required for cytochrome oxidase assembly, *J. Biol. Chem. 279*, 49883-49888.

29. Palumaa, P., Kangur, L., Voronova, A., and Sillard, R. (2004) Metal-binding mechanism of Cox17, a copper chaperone for cytochrome *c* oxidase, ***Biochem. J.*** ***382***, 307-314.

30. Hiser, L., Di Valentin, M., Hamer, A. G., and Hosler, J. P. (2000) Cox11p is required for stable formation of the Cu_B and magnesium centers of cytochrome *c* oxidase, ***J. Biol. Chem.*** ***275***, 619-623.

31. Luk, E., Jensen L. T., and Culotta, V. C. (2003) The many highways for intracellular trafficking of metals, ***J. Biol. Inorg. Chem***. ***8***, 803-809.

32. Crichton, R. R., and Pierre, J.-L. (2001) Old iron, young copper: From Mars to Venus, ***Biometals*** ***14***, 99-112.

33. Berg, Jeremy M., Tymoczko, John L., and Stryer, Lubert (2002) ***Biochemistry***, 5th ed., W. H. Freeman and Company, New York.

34. Skirry, J. (2005) ***Descartes and the metaphysics of human nature***, Continuum Press, London.

35. Figgis, B. N., and Hitchman, M. A. (2000) "Ligand field theory and its applications", Wiley-VCH Publishers, New York.

36. Lin, C. I. P., Ohnishi, T., Clejan, L., and Beattie, D. S. (1983) The presence of the iron-sulfur protein (subunit V) of complex III in mitochondria of heme-deficient yeast cells lacking iron-sulfur clusters detectable by electron paramagnetic resonance, ***Eur. J. Biochem***. ***137***, 179-183.

37. Hunter, D. J. B., Salerno, J. C., and Ingledew, W. J. (1998) Angular dependence of electron paramagnetic resonances of an azide-NO complex of cytochrome *c*

oxidase: Orientation of the [heme]-copper axis in cytochrome aa_3 from ox heart, *BBA-Bioenergetics 1364*, 55-62.

38. Boumans, H., van Gaalen, M. C. M., Grivell, L. A., and Berden, J. A. (1997) Differential inhibition of the yeast bc_1 complex by phenanthrolines and ferroin: Implications for structure and catalytic mechanism, *J. Biol. Chem. 272*, 16753-16760.

39. Ramabadran, R. S., Japa, S., and Beattie, D. S. (1997) Assembly of deletion mutants of the Rieske iron-sulfur protein into the cytochrome bc_1 complex of yeast mitochondria, *Journal of Bioenergetics and Biomembranes 29*, 45-54.

40. Pershad, H. R., Hirst, J., Cochran, B., Ackrell, B. A. C., and Armstrong, F. A. (1999) Voltammetric studies of bidirectional catalytic electron transport in *Escherichia coli* succinate dehydrogenase: Comparison with the enzyme from beef heart mitochondria, *BBA-Bioenergetics 1412*, 262-272.

41. Cammack, R., Gay, E., and Shergill, J. K. (1999) Studies of hyperfine interactions in [2Fe-2S] proteins by EPR and double resonance spectroscopy, *Coordination Chemistry Reviews 192*, 1003-1022.

42. Megli, F. M., and Sabatini, K. (2003) Respiration state IV-generated ROS destroy the mitochondrial bilayer packing order *in vitro*: An EPR study, *FEBS Letts. 550*, 185-189.

43. Gabbita, S. P., Subramaniam, R., Allouch, F., Carney, J. M., and Butterfield, D. A. (1998) Effects of mitochondrial respiratory stimulation on membrane lipids

and proteins: An electron paramagnetic resonance investigation, *BBA-Biomembranes 1372*, 163-173.

44. Vavrinkova, H., Tutterova, M., Stopka, P., Kazdova, L., and Drahota, Z. (2001) The effect of captopril on nitric oxide formation and on generation of radical forms of mitochondrial respiratory chain compounds in ischemic rat heart, *Physiological Research 50*, 481-489.

45. Green, D. E., and Vande Zande, H. (1982) On the enzymic mechanism of oxidative phosphorylation, *Proc. Natl. Acad. Sci. 79*, 1064-1068.

46. Sharp, R. E., White, P., Chapman, S. K., and Reid, G. A. (1994) Role of the interdomain hinge of flavocytochrome b_2 in intraprotein and interprotein electron transfer, *Biochemistry 33*, 5115-5120.

47. Arscott, L. D., Gromer, S., Schirmer, R. H., Becker, K., and Williams, C. H. (1997) The mechanism of thioredoxin reductase from human placenta is similar to the mechanisms of lipoamide dehydrogenase and glutathione reductase and is distinct from the mechanism of thioredoxin reductase from *Escherichia* coli, *Proc. Natl. Acad. Sci. 94*, 3621-3626.

48. Staples, C. R., Ameyibor, E., Fu, W. G., Gardet-Salvi, L., Stritt-Etter, E. L., Knaff, D. B., and Johnson, M. K. (1996) The functional properties of the iron-sulfur center in spinach ferredoxin-thioredoxin reductase: A new biological role for iron-sulfur clusters, *Biochemistry 35*, 11425-11434.

49. Garrib, A., and McMurray, W. C. (1986) Purification and characterization of glycerol-3-phosphate dehydrogenase (flavin-linked) from rat liver mitochondria, *J. Biol. Chem. 261*, 8042-8048.

50. Huh, W. K., Kim, S. T., Yang, K. S., Seok, Y. J., Hah, Y. C., and Kang, S. O. (1994) Characterization of *D*-arabinono-1,4-lactone oxidase from *Candida albicans* ATCC-10231, *European Journal of Biochemistry 225*, 1073-1079.

51. Joo, H. S., and Kim, S. S. (1998) Purification and characterization of the catabolic α-acetolactate synthase from *Serratia marcescens*, *Journal of Biochemistry and Molecular Biology 31*, 37-43.

52. Shan, X. Y., Wang, L. Q., Hoffmaster, R., and Kruger, W. D. (1999) Functional characterization of human methylenetetrahydrofolate reductase in *Saccharomyces cerevisiae*, *J. Biol. Chem. 274*, 32613-32618.

53. Robinson, K. M., and Lemire, B. D. (1996) A requirement for matrix processing peptidase but not for mitochondrial chaperonin in the covalent attachment of FAD to the yeast succinate dehydrogenase flavoprotein, *J. Biol. Chem. 271*, 4061-4067.

54. Gin, P., Hsu, A. Y., Rothman, S. C., Jonassen, T., Lee, P. T., Tzagoloff, A., and Clarke, C. F. (2003) The *Saccharomyces cerevisiae COQ*6 gene encodes for a mitochondrial flavin-dependent monooxygenase required for coenzyme Q biosynthesis, *J. Biol. Chem. 278*, 25308-25316.

55. Oxelmark, E., Marchini, A., Malanchi, I., Magherini, F., Jaquet, L., Hajibagheri, M. A. N., Blight, K. J., Jauniaux, J. C., and Tommasino, M. (2000) Mmf1p, a

novel yeast protein conserved throughout evolution and involved in maintenance of the mitochondrial genome, *Molecular and Cellular Biology 20*, 7784-7797.

56. Aleksandrov, A. Y., Druzhenkov, V. V., Ivanov, I. I., Kuzmin, R. N., Novakova, A. A., Rubin, A. B., and Sjemin, B. K. (1979) Study of accumulation of iron by the isolated rat liver mitochondria by Mössbauer spectroscopy, *Biofizika 24*, 663-665.

57. Tong, W. H., Jameson, G. N. L., Huynh, B. H., and Rouault, T. A. (2003) Subcellular compartmentalization of human Nfu, an iron-sulfur scaffold protein, and its ability to assemble a [4Fe-4S] cluster, *Proc. Natl. Acad. Sci. USA 100*, 9762-9767.

58. Lillig, C. H., Berndt, C., Vergnolle, O., Lonn, M. E., Hudemann, C., Bill, E., and Holmgren, A. (2005) Characterization of human glutaredoxin 2 as an iron-sulfur protein: A possible role as redox sensor, *Proc. Natl. Acad. Sci. USA 102*, 8168-8173.

59. Lesuisse, E., Santos, R., Matzanke, B. F., Knight, S. A. B., Camadro, J. M., and Dancis, A. (2003) Iron use for [heme] synthesis is under control of the yeast frataxin homologue (Yfh1), *Hum. Mol. Gen. 12*, 879-889.

60. Diekert, K., de Kroon, A. I. P. M., Kispal, G., and Lill, R. "Isolation and subfractionation of mitochondria from the yeast *Saccharomyces cerevisiae*" in *Methods in Yeast Genetics*, vol. 65. Liza A. Pon and Eric A. Schon, eds. Academic Press, San Diego, 2000.

61. M. J. Nilges, Ph.D dissertation, University of Illinois, Urbana, Illinois, 1979; R. L. Bedford and M. J. Nilges. Computer simulation of powder spectra, 21st Rocky Mountain Conference, Denver, CO, August 1979; A. M. Maurice, Ph.D. dissertation, University of Illinois, Urbana, Illinois, 1980.

62. Orme-Johnson, N. R., and Orme-Johnson, W. H. in *Methods in Enzymology*, vol. 52, pp. 252-257. Academic Press, New York, 1978.

63. Wright, R. (2000) Transmission electron microscopy of yeast, *Microscopy Research and Technique 51*, 496-510.

64. Dineley, K. E., Richards L. L., Votyakova, T. V., and Reynolds, I. J. (2005) Zinc causes loss of membrane potential and elevates reactive oxygen species in rat brain mitochondria, *Mitochondria 5*, 55-65.

65. Lund, P., and Wiggins, D. (1990) Maintenance of energy-linked functions in rat liver mitochondria, *BBA 1018*, 98-102.

66. Cleland, W. W. (1964) Dithiothreitol, a new protective reagent for SH groups, *Biochemistry 3*, 480.

67. Barondeau, D. P., Roberts, L. M., and Lindahl, P. A. (1994) "Stability of the Ni-C state and oxidative titrations of the nickel hydrogenase from *Desulfovibrio gigas* monitored by EPR and electronic absorption spectroscopies, *J. Am. Chem. Soc*. *116*, 3442 - 3448.

68. Hackenbrock, C. R. (1968) Ultrastructural bases for metabolically linked mechanical activity in mitochondria, *The Journal of Cell Biology 37*, 345-369.

69. Shaw, J. M., and Nunnari, J. (2002) Mitochondrial dynamics and division in budding yeast, *Trends in Cell Bio*. *12*, 178-184.

70. Egner, A., Jakobs, S., and Hell, S. W. (2002) Fast 100-nm resolution three-dimensional microscope reveals structural plasticity of mitochondria in live yeast, *Proc. Natl. Acad. Sci. USA 99*, 3370-3375.

71. Sapan, C. V., Lundlad, R. L., and Price, N. C. (1999) Colorimetric protein assay techniques, *Biotechnology and Applied Biochemistry 29*, 99-108.

72. Lindahl, P. A., Day, E. P., Kent, T. A., Orme-Johnson, W. H., and Münck, E. (1985) Mössbauer, EPR, and magnetization studies of the *Azobacter vinelandii* Fe protein. Evidence for a $[4Fe\text{-}4S]^{+}$ cluster with spin $S = 3/2$, *J. Biol. Chem. 260*, 11160.

73. Huston, W. M., Andrew, C. R., Servid, A. E., McKay, A. L., Leech, A. P., Butler, C. S., and Moir, J. W. B. (2006) Heterologous overexpression and purification of cytochrome *c′* from *Rhodobacter capsulatus* and a mutant (K42E) in the dimerization region. Mutation does not alter oligomerization but impacts the heme iron spin state and nitric oxide binding properties, *Biochemistry 45*, 4388-4395.

74. Mayhew, S. G. (1978) Redox potential of dithionite and SO_2^- from equilibrium reactions with flavodoxins, methyl viologen and hydrogen plus hydrogenase, *European Journal of Biochemistry 85*, 535-547.

75. Huang, L. S., Cobessi, D., Tung, E. Y., and Berry, E. A. (2005) Binding of the respiratory chain inhibitor antimycin to the mitochondrial bc_1 complex: A new

crystal structure reveals an altered intramolecular hydrogen-bonding pattern, *Journal of Molecular Biololgy 351*, 573-597.

76. Terauchi, S., Yamamoto, T., Yamashita, K., Kataoka, M., Terada, H., and Shinohara, Y. (2005) Molecular basis of morphological changes in mitochondrial membrane accompanying induction of permeability transition, as revealed by immuno-electron microscopy, *Mitochondrion 5*, 248-254.

77. Cobine, P. A., Ojeda, L. D., Rigby, K. M., and Winge D. R. (2004) Yeast contain a non-proteinaceous pool of copper in the mitochondrial matrix, *J. Biol. Chem. 279*, 14447-14455.

78. Ghaemmaghami, S., Huh, W. K., Bower, K., Howson, R. W., Belle, A, Dephoure, N., O'Shea, E. K., and Weissman, J. S. (2003) Global analysis of protein expression in yeast, *Nature* 425, 737-741.

79. Agar, J. N., Krebs, C., Frazzon, J., Huynh, B. H., Dean, D. R., and Johnson, M. K. (2000) IscU as a scaffold for iron-sulfur cluster biosynthesis: Sequential assembly of [2Fe-2S] and [4Fe-4S] clusters in IscU, *Biochemistry 39*, 7856-7862.

80. Lange, H., Kispal, G., and Lill, R. Mechanism of iron transport to the site of heme synthesis inside yeast mitochondria, *J. Biol. Chem. 274*, 18989-18996.

81. Ollagnier-de Choudens, S., Sanakis, Y., Hewitson, K. S., Roach, P., Baldwin, J. E., Münck, E., and Fontecave, M. (2000) Iron-sulfur center of biotin synthase and lipoate synthase, *Biochemistry 39*, 4165-4173.

82. Franco, R., Moura, J. J. G., Moura, I., Huynh, B. H., Forbes, W. S., and Ferreira, G. C. (1995) Characterization of the iron binding site in mammalian

ferrochelatase by kinetic and Mössbauer methods, *J. Biol. Chem. 270*, 26352-26357.

83. Haile, D. J., Rouault, T. A., Harford, J. B., Kennedy, M. C., Blondin, G. A., Beinert, H., and Klausner, R. D. (1992) Cellular regulation of the iron responsive element binding protein- disassembly of the cubane iron-sulfur cluster results in high-affinity RNA binding, *Proc. Natl. Acad. Sci. USA 89*, 11735-11739.

84. Henze, K., Martin, W. (2003) Essence of mitochondria, *Nature 426*, 127-128.

85. Mühlenhoff, U., and Lill, R. (2000) Biogenesis of iron-sulfur proteins in eukaryotes: A novel task of mitochondria that is inherited from bacteria, *Biochimica et Biophysica Acta-Bioenergetics 1459*, 370-382.

86. Jackson, T. A., Karapetian, A., Miller, A. F., and Brunold, T. C. (2004) Spectroscopic and computational studies of the azide-adduct of manganese superoxide dismutase: Definitive assignment of the ligand responsible for the low-temperature thermochromism, *J. Am. Chem. Soc. 126*, 12477-12491.

87. Un, S., Tabares, L. C., Cortez, N., Hiraoka, B. Y., and Yamakura, F. (2004) Manganese(II) zero-field interaction in cambialistic and manganese superoxide dismutases and its relationship to the structure of the metal binding site, *J. Am. Chem. Soc. 126*, 2720-2726.

88. Werth, M. T., Sices, H., Cecchini, G., Schroder, I., Lasage, S., Gunsalus, R. P., and Johnson, M. K. (1992) Evidence for non-cysteinyl coordination of the [2Fe-2S] cluster in *Escherichia coli* succinate dehydrogenase, *FEBS Letters 299*, 1-4.

89. Srinivasan, C., Liba, A., Imlay, J. A., Valentine, J. S., and Gralla, E. B. (2000) Yeast lacking superoxide dismutase(s) show elevated levels of "free iron" as measured by whole cell electron paramagnetic resonance, *J. Biol. Chem. 275*, 29187-29192.

90. Werth, M. T., Sices, H., Cecchini, G., Schroder, I., Lasage, S., Gunsalus, R. P., and Johnson, M. K. (1992) Evidence for non-cysteinyl coordination of the [2Fe-2S] cluster in *Escherichia coli* succinate dehydrogenase, *FEBS Letters 299*, 1-4.

91. Shergill J. K., Cammack R., Chen J. H., Fisher, M. J., Madden, S., and Rees, H. H. (1995) EPR spectroscopic characterization of the iron-sulfur proteins and cytochrome P450 in mitochondria from the insect *Spodoptera littoralis* (cotton leafworm), *Biochemical Journal 307*, 719-728.

92. Fee, J. A., Findling, K. L, Yoshida, T., Hille, R., Tarr, G. E., Hearshen, D. O., Dunham, W. R., Day, E. P., Kent, T. A., and Münck, E. (1984) Purification and characterization of the Rieske iron-sulfur protein from *Thermus thermophilus* – Evidence for a [2Fe-2S] cluster having non-cysteine ligands, *J. Biol. Chem. 259*, 124-133.

93. Hirst, J., Sucheta, A., Ackrell, B. A. C., and Armstrong, F. A. (1996) Electrocatalytic voltammetry of succinate dehydrogenase: Direct quantification of the catalytic properties of a complex electron-transport enzyme, *J. Am. Chem. Soc. 118*, 5031-5038.

94. Sucheta, A., Ackrell, B. A. C., Cochran, B., and Armstrong, F. A. (1992) Diode-like [behavior] of a mitochondrial electron-transport enzyme, *Nature 356*, 361-362.

95. Link, T. A., Hagen, W. R., Pierik, A. J., Assmann, C., and von Jagow, G. (1992) Determination of the redox properties of the Rieske [2Fe-2S] cluster of bovine heart bc_1 complex by direct electrochemistry of a water-soluble fragment, *Eur. J. Biochem. 208*, 685-691.

96. Kilpatrick, L. K., Kennedy, M. C., Beinert, H., Czernuszewicz, R. C., Qiu, D., and Spiro, T.G. (1994) Cluster structure and H-bonding in native, substrate-bound, and 3Fe forms of aconitase as determined by resonance Raman spectroscopy, *J. Am. Chem. Soc. 116*, 4053-4061.

97. Ruzicka, F. J., Beinert, H., Schepler, K. L., Dunham, W. R., Sands, R. H. (1975) Interaction of ubisemiquinone with a paramagnetic component in heart tissue, *Proc. Natl. Acad. Sci. USA 72*, 2886-2890.

98. Beinert, H., and Shaw, R. W. (1977) On identity of high-spin heme components of cytochrome *c* oxidase, *Biochimica et Biophysica Acta 462*, 121-130.

99. Leigh, J. S., and Wilson, D. F. (1972) Heme-heme interactions in cytochrome *c* oxidase – effects of photodissociation of CO compound, *Biochemical and Biophysical Research Communications 48*, 1266.

100. Wittenberg, B. A., Kampa, L., Wittenberg, J. B., Blumberg, W. E., and Peisach, J. (1968) The electronic structure of protoheme proteins, *J. Biol. Chem. 243*, 1863-1870.

101. Coulson, A. F. W., Erman, J. E., and Yonetani, T. (1971) Studies on cytochrome *c* peroxidase, *J. Biol. Chem. 246*, 917-924.

102. Goodin, D. B., Mauk, A. G., and Smith, M. (1987) The peroxide complex of yeast cytochrome *c* peroxidase contains two distinct radical species, neither of which resides at methionine 172 or tryptophan 51, *Biochemistry 262*, 7719-7724.

103. Goodin, D. B., and McRee, D. E. (1993) The Asp-His-Fe triad of cytochrome *c* peroxidase controls the reduction potential, electronic structure, and coupling of the tryptophan free radical to the heme, *Biochemistry 32*, 3313-3324.

104. Lester, R. L., and Crane, F. L. (1959) The natural occurrence of coenzyme Q and related compounds, *J. Biol. Chem. 234*, 2169-2175.

105. Fontecave, M., Ollagnier-de-Choutens, S., Mulliez, E. (2003) Biological radical sulfur insertion reactions, *Chem. Rev. 103,* 2149-2166.

106. Maguire, J. J., Johnson, M. K., Morningstar, J. E., Ackrell, B. A. C., and Kearney, E. B. (1985) Electron paramagnetic studies of mammalian succinate dehydrogenase, *J. Biol. Chem. 260*, 10909-10912.

107. Nicholls, P., and Elliott, W. B. "The cytochromes" in *Iron in biochemistry and medicine*, Worwood, M. and Jacobs, A., eds. Academic Press, New York, 1974.

108. Lett, C. M., and Guillemette, J. G. (2002) Increasing the redox potential of isoform 1 of yeast cytochrome *c* through the modification of select heme interactions, *Biochemical J. 362*, 281-287.

109. Anemüller, S., Bill, E., Schäfer, G., Trautwein, A., and Teixeira, M. (1992) EPR study of cytochrome aa_3 from *Sulfolobus acidocaldarius*, *Eur. J. Biochem. 210*, 133-138.

110. Beinert, H., and Shaw, R. W. (1977) On identity of high-spin heme components of cytochrome *c* oxidase, *Biochimica et Biophysica Acta 462*, 121-130.

111. Merbitz-Zahradnik, T., Zwicker, K., Nett, J. H., Link, T. A., and Trumpower, B. L. (2003) Elimination of the disulfide bridge in the Rieske iron-sulfur protein allows assembly of the [2Fe-2S] cluster into the Rieske protein but damages the ubiquinol oxidation site in the cytochrome bc_1 complex, *Biochemistry 42*, 13637-13645.

112. Gavin, C. E., Gunter, K. K., and Gunter, T. E. (1999) Manganese and calcium transport in mitochondria: Implications for manganese toxicity, *Neurotoxicology 20*, 445-453.

113. Tuckey, R. C., McKinley, A. J., and Headlam, M. J. (2001) Oxidized adrenodoxin acts as a competitive inhibitor of cytochrome P450scc in mitochondria from the human placenta, *Eur. J. Biochem. 268*, 2338-2343.

114. Guldutuna, S., Zimmer, G., Leuschner, M., Bhatti, S., Elze, A., Beisinger, B., Hofmann, M., and Leuschner, U. (1999) The effect of bile salts and calcium on isolated rat liver mitochondria, *Biochim. Biophys. Acta 1453*, 396-406.

115. Shergill, J. K., and Cammack, R. (1994) ESEEM studies of the iron-sulfur clusters of succinate dehydrogenase in arum-maculatum spadix mitochondrial membranes, *Biochim. Biophys. Acta 1185*, 43-49.

116. Münck, E., Surerus, K. K., and Hendrich, M. P. (1993) Combining Mössbauer spectroscopy with integer spin electron paramagnetic resonance, *Methods in Enzymology 227*, 463-479.

APPENDIX I

QPOWA PARAMETERS FOR SIMULATING EPR SIGNALS

The following parameters were used to simulate the spectrum shown in Chapter III, Figure 3-5:

1) Parameters for g_{ave} = 2.04 signal:

```
bnhg204iso12.out
bnhg204iso12.txt
QPOWA - g2.04 test
  9.41400  1
     0.0     0.0     0.0     0.0       0       0       0
      14      30      10       0       1       1
    75.00   80.00   80.00     4.0       1
    0.0 0.0 0.0  0.0 0.0 0.0
    0.0 0.0 0.0
    0.0   0.0    0.0  1.0  1
    3550.1465    900.293    0.9761388
  2.08500 2.02100 2.00700
    60.01   60.01   60.00     0.0     0.0     0.0
    25.00    9.00   87.00     0.0     0.0     0.0
    0.00    0.00    0.00     0.0     0.0     0.0
    0.00    0.00    0.00     0.0     0.0     0.0
    18.64   12.79            0.0     0.0     0.0
```

2) Parameters for g_{ave} = 1.94 signal:

```
bnhsdh2.out
bnhsdh2.txt
QPOWA – 2Fe-2S test
  9.41400  1
     0.0     0.0     0.0     0.0       0       0       0
      16      40      10       0       1       1
    34.00   30.00   34.00     4.0       1
    0.0 0.0 0.0  0.0 0.0 0.0
    0.0 0.0 0.0
    0.0   0.0    0.0  1.0  1
    3550.1465    900.293    0.9761388
  2.02600 1.93400 1.913000
    60.01   60.01   60.00     0.0     0.0     0.0
    25.00    9.00   87.00     0.0     0.0     0.0
    0.00    0.00    0.00     0.0     0.0     0.0
```

```
  0.00    0.00    0.00     0.0     0.0     0.0
 18.64   12.79            0.0     0.0     0.0
```

3) Parameters for g_{ave} = 1.90 signal:

```
bnhrsknew4.out
bnhrsknew4.txt
QPOWA – 2Fe-2S test
  9.41400  1
     0.0     0.0     0.0     0.0       0       0       0
      16      40      10       0       1       1
   200.00   70.00   24.00      4.0       1
    0.0 0.0 0.0  0.0 0.0 0.0
    0.0 0.0 0.0
    0.0   0.0    0.0  1.0  1
    3550.1465    900.293    0.9761388
  2.02500 1.89700 1.78400
   60.01   60.01   60.00     0.0     0.0     0.0
   25.00    9.00   87.00     0.0     0.0     0.0
    0.00    0.00    0.00     0.0     0.0     0.0
    0.00    0.00    0.00     0.0     0.0     0.0
   18.64   12.79            0.0     0.0     0.0
```

4) Parameters for g_{ave} = 2.00 signal:

```
bnhrad45.out
bnhrad45.txt
QPOWA - Radical
  9.41400  1
     0.0     0.0     0.0     0.0       0       0       0
      16      40       2       0       1       1
   13.00    13.00    13.00      4.0       1
    0.0 0.0 0.0  0.0 0.0 0.0
    0.0 0.0 0.0
    0.0   0.0    0.0  1.0  1
    3350.00    700.00    0.6835938
  2.00000 2.00000 2.00000
   60.01   60.01  420.00     0.0     0.0     0.0
   25.00    9.00   87.00     0.0     0.0     0.0
    0.00    0.00    0.00     0.0     0.0     0.0
    0.00    0.00    0.00     0.0     0.0     0.0
```

```
    18.64   12.79            0.0     0.0     0.0
```

The following parameters were used to simulate the spectrum shown in Chapter III, Figure 3-7:

1) Parameters for g_{ave} = 2.04 signal:

```
bnhg204iso32.out
bnhg204iso32.txt
QPOWA - g2.04 test
  9.48400  1
     0.0     0.0     0.0     0.0       0       0       0
      14      30      10       0       1       1
    70.00   80.00   50.00      4.0      1
    0.0 0.0 0.0  0.0 0.0 0.0
    0.0 0.0 0.0
    0.0   0.0    0.0  1.0  1
    3550.1465    900.293    1.4639
  2.10300 2.02500 2.01000
    60.01   60.01   60.00     0.0     0.0     0.0
    25.00    9.00   87.00     0.0     0.0     0.0
     0.00    0.00    0.00     0.0     0.0     0.0
     0.00    0.00    0.00     0.0     0.0     0.0
    18.64   12.79            0.0     0.0     0.0
```

2) Parameters for g_{ave} = 1.94 signal:

```
sdh92.out
sdh92.txt
QPOWA - 2Fe-2S test
  9.48400  1
     0.0     0.0     0.0     0.0       0       0       0
      16      40      10       0       1       1
    34.00   30.00   34.00      4.0      1
    0.0 0.0 0.0  0.0 0.0 0.0
    0.0 0.0 0.0
    0.0   0.0    0.0  1.0  1
    3550.1465    900.293    1.4639
  2.02600 1.93400 2.01000
    60.01   60.01   60.00     0.0     0.0     0.0
    25.00    9.00   87.00     0.0     0.0     0.0
     0.00    0.00    0.00     0.0     0.0     0.0
```

```
  0.00    0.00    0.00     0.0     0.0     0.0
 18.64   12.79            0.0     0.0     0.0
```

3) Parameters for g_{ave} = 1.90 signal:

```
rsknew2.out
rsknew2.txt
QPOWA – 2Fe-2S test
  9.48400  1
     0.0     0.0     0.0     0.0       0       0       0
      16      40      10       0       1       1
   24.00   60.00   200.00      4.0       1
    0.0 0.0 0.0  0.0 0.0 0.0
    0.0 0.0 0.0
    0.0   0.0    0.0  1.0  1
    3550.1465    900.293    1.4639
  2.02600 1.89700 1.78400
   60.01   60.01   60.00     0.0     0.0     0.0
   25.00    9.00   87.00     0.0     0.0     0.0
    0.00    0.00    0.00     0.0     0.0     0.0
    0.00    0.00    0.00     0.0     0.0     0.0
   18.64   12.79            0.0     0.0     0.0
```

4) Parameters for g_{ave} = 2.00 signal:

```
rad18.out
rad18.txt
QPOWA - Radical
  9.48400  1
     0.0     0.0     0.0     0.0       0       0       0
      16      40       2       0       1       1
   12.00    12.00    12.00      4.0       1
    0.0 0.0 0.0  0.0 0.0 0.0
    0.0 0.0 0.0
    0.0   0.0    0.0  1.0  1
    3550.1465    900.293    1.4639
  2.00230 2.00230 2.00230
   60.01   60.01  420.00     0.0     0.0     0.0
   25.00    9.00   87.00     0.0     0.0     0.0
    0.00    0.00    0.00     0.0     0.0     0.0
    0.00    0.00    0.00     0.0     0.0     0.0
```

18.64 12.79 0.0 0.0 0.0

5) Parameters for g_{ave} = 2.02 signal:

shelleysig06.out
shelleysig06.txt
QPOWA – g2.02
9.48400 1
0.0 0.0 0.0 0.0 0 0 0
16 40 2 0 1 1
12.00 100.00 25.00 4.0 1
0.0 0.0 0.0 0.0 0.0 0.0
0.0 0.0 0.0
0.0 0.0 0.0 1.0 1
3550.1465 900.293 1.4639
2.02600 2.02200 2.00030
60.01 60.01 420.00 0.0 0.0 0.0
25.00 9.00 87.00 0.0 0.0 0.0
0.00 0.00 0.00 0.0 0.0 0.0
0.00 0.00 0.00 0.0 0.0 0.0
18.64 12.79 0.0 0.0 0.0

The following parameters were used to simulate the air-oxidized spectrum shown in Chapter III, Figure 3-3:

1) Parameters for the g = 2.01 signal:

1Dec04Aco117.out
1Dec04Aco117.txt
QPOWA - 2Fe-2S test
9.41900 1
0.0 0.0 0.0 0.0 0 0 0
16 40 10 0 1 1
20.50 33.00 33.00 4.0 1
0.0 0.0 0.0 0.0 0.0 0.0
0.0 0.0 0.0
0.0 0.0 0.0 1.0 1
3600.0000 1000.000 0.9765625
1.99670 2.01400 2.01900
60.01 60.01 60.00 0.0 0.0 0.0
25.00 9.00 87.00 0.0 0.0 0.0
0.00 0.00 0.00 0.0 0.0 0.0
0.00 0.00 0.00 0.0 0.0 0.0

```
    18.64   12.79            0.0     0.0     0.0
```

2) Parameters for the g = 1.94 signal:

```
1Dec04Sdh110.out
1Dec04Sdh110.txt
QPOWA - 2Fe-2S test
  9.41900  1
     0.0     0.0     0.0     0.0       0       0       0
      16      40      10       0       1       1
    42.00   33.00   34.00      4.0       1
    0.0 0.0 0.0  0.0 0.0 0.0
    0.0 0.0 0.0
    0.0   0.0    0.0  1.0  1
    3600.0000    1000.000    0.9765625
  1.91330 1.93150 2.026000
    60.01   60.01   60.00     0.0     0.0     0.0
    25.00    9.00   87.00     0.0     0.0     0.0
    0.00    0.00    0.00     0.0     0.0     0.0
    0.00    0.00    0.00     0.0     0.0     0.0
    18.64   12.79            0.0     0.0     0.0
```

3) Parameters for the g = 1.90 signal:

```
1Dec04Rip119.out
1Dec04Rip119.txt
QPOWA - 2Fe-2S test
  9.41900  1
     0.0     0.0     0.0     0.0       0       0       0
      16      40      10       0       1       1
   102.00   64.00   12.00      4.0       1
    0.0 0.0 0.0  0.0 0.0 0.0
    0.0 0.0 0.0
    0.0   0.0    0.0  1.0  1
    3600.0000    1000.000    0.9765625
  1.78190 1.89300 2.02660
    60.01   60.01   60.00     0.0     0.0     0.0
    25.00    9.00   87.00     0.0     0.0     0.0
    0.00    0.00    0.00     0.0     0.0     0.0
    0.00    0.00    0.00     0.0     0.0     0.0
    18.64   12.79            0.0     0.0     0.0
```

The following parameters were used to simulate the ferricyanide-oxidized spectrum shown in Chapter III, Figure 3-3:

1) Parameters for the g = 2.00 (isotropic) signal:

```
8Feb06Rad04.out
8Feb06Rad04.txt
QPOWA - 2Fe-2S test
  9.44800  1
     0.0     0.0     0.0     0.0       0       0       0
      16      40      10       0       1       1
    16.00   16.00   16.00      4.0      1
    0.0 0.0 0.0  0.0 0.0 0.0
    0.0 0.0 0.0
    0.0   0.0    0.0  1.0  1
    3350.0000    700.000    0.6835975
  2.00720 2.00720 2.00720
   60.01   60.01   60.00     0.0     0.0     0.0
   25.00    9.00   87.00     0.0     0.0     0.0
    0.00    0.00    0.00     0.0     0.0     0.0
    0.00    0.00    0.00     0.0     0.0     0.0
   18.64   12.79            0.0     0.0     0.0
```

2) Parameters for the g = 2.01 signal:

```
8Feb0640dBAco124.out
8Feb0640dBAco124.txt
QPOWA - 2Fe-2S test
  9.44800  1
     0.0     0.0     0.0     0.0       0       0       0
      16      40      10       0       1       1
    20.00   43.00   31.00      4.0      1
    0.0 0.0 0.0  0.0 0.0 0.0
    0.0 0.0 0.0
    0.0   0.0    0.0  1.0  1
    3350.0000    700.000    0.6835975
  1.99150 2.01000 2.02350
   60.01   60.01   60.00     0.0     0.0     0.0
   25.00    9.00   87.00     0.0     0.0     0.0
    0.00    0.00    0.00     0.0     0.0     0.0
    0.00    0.00    0.00     0.0     0.0     0.0
   18.64   12.79            0.0     0.0     0.0
```

APPENDIX II

BIOCHEMICAL AND PHYSICAL DATA FOR MITOCHONDRIAL METALLOPROTEINS IN *SACCHAROMYCES CEREVISIAE*

Table A1. Localization and reduction potentials of potential contributors to the EPR spectra of whole mitochondria from *Saccharomyces cerevisiae*.

Cofactor	**Protein**	**Location**	***E*°´(mV) vs NHE**	**References**
Aco1p $[4Fe\text{-}4S]^{+2/+1}$	Aco1p	Matrix	$E°$ = -450	145
Sdh2p $[2Fe\text{-}2S]^{+2/+1}$	Succinate dehydrogenase	Inner membrane, matrix side	$E°$ = 0	139, 140
Sdh2p $[3Fe\text{-}4S]^{+1/0}$	Succinate dehydrogenase	Inner membrane, matrix side	$E°$ = +60	139, 140
Sdh2p $[4Fe\text{-}4S]^{+2/+1}$	Succinate dehydrogenase	Inner membrane, matrix side	$E°$ = -260	139, 140
Rip1p $[2Fe\text{-}2S]^{+2/+1}$	Cytochrome bc_1	Inner membrane, IMS side	$E°$ = +270	50
Heme $b_{562}^{3+/2+}$	Cytochrome bc_1	Inner membrane	$E°$ = -167	141
Heme $b_{566}^{3+/2+}$	Cytochrome bc_1	Inner membrane IMS side	$E°$ = -30	138
Heme $c_1^{3+/2+}$	Cytochrome bc_1	Inner membrane	$E°$ = +340	143
Heme $c^{3+/2+}$	Cytochrome *c*	Inner membrane, IMS side	$E°$ = +260	142
Heme $a^{3+/2+}$	Cytochrome oxidase	Inner membrane	$E°$ = +255	135
Heme $a_3^{3+/2+}$	Cytochrome oxidase	Inner membrane	$E°$ = +190	135
$Cu_A^{2+/+1}$	Cytochrome oxidase	Inner membrane	$E°$ = +240	136
$Cu_B^{2+/+1}$	Cytochrome oxidase	Inner membrane	$E°$ = +370	135
Coenzyme Q (ubiquinone)	N/A	Inner membrane	$E°$ = +45	138
$FADH_2$	N/A	Intermembrane space, matrix	$E°_1$ = -128 $E°_2$ = -30	139

Table A-2. Estimated range of concentrations of cytochrome proteins in EPR samples given at 50 mg/mL. Estimated concentrations were taken from Nicholls, P., and Elliott, W. B. "The cytochromes" in "Iron in biochemistry and medicine", Worwood, M. and Jacobs, A., eds. Academic Press, New York, 1974.

Protein	**Estimated concentration (µmol/g protein)**	**Concentration at 50 mg/mL protein (µM)**
Cytochrome $a + a_3$	0.15-0.3	7.5-15
Cytochrome *b*	0.3-0.4	15-20
Cytochrome *c*	0.2-0.4	10-20
Cytochrome c_1	0.07-0.25	3.5-12.5

VITA

Brandon Neal Hudder was raised in Douglasville, GA. He is the son of Barry and Nancy Hudder and is a proud graduate of Alexander High School. After receiving his bachelor's degree from the University of West Georgia, he moved to Texas in May 2000 and began his graduate career at Texas A&M University.

Dr. Hudder may be reached via e-mail at bnhudder@medlencarroll.com through the firm of Medlen & Carroll, LLP, San Francisco, CA.